Self-assembling nanoparticles presenting receptor binding domain and stabilized spike as next-generation COVID-19 vaccines

Linling He[1], Xiaohe Lin[1], Ying Wang[4,5], Ciril Abraham[4], Cindy Sou[1], Timothy Ngo[1], Yi Zhang[4,5], Ian A. Wilson[1,3], and Jiang Zhu[1,2*]

[1]Department of Integrative Structural and Computational Biology, [2]Department of Immunology and Microbiology, [3]Skaggs Institute for Chemical Biology, The Scripps Research Institute, La Jolla, California 92037, USA

[4]Fels Institute for Cancer Research and Molecular Biology, and [5]Department of Microbiology and Immunology, Temple University, Philadelphia, Pennsylvania 19140, USA.

[*] Corresponding author (to whom correspondence should be addressed)

JZ: Phone (858) 784-8157; Email: jiang@scripps.edu

KEYWORDS

Coronavirus disease 2019 (COVID-19); heptad repeat 2 (HR2); self-assembling protein nanoparticle (SApNP); severe acute respiratory syndrome coronavirus 2 (SARS-CoV-2); spike (S) protein; vaccine.

ABSTRACT (150 words)

We present a comprehensive vaccine strategy for severe acute respiratory syndrome coronavirus 2 (SARS-CoV-2) by combining antigen optimization and nanoparticle display. We first developed a receptor binding domain (RBD)-specific antibody column for purification and displayed the RBD on self-assembling protein nanoparticles (SApNPs) using the SpyTag/SpyCatcher system. We then identified the heptad repeat 2 (HR2) stalk as a major cause of spike metastability, designed an HR2-deleted glycine-capped spike (S2GΔHR2), and displayed S2GΔHR2 on three SApNPs with high yield, purity, and antigenicity. Compared to the RBD, the RBD-ferritin SApNP elicited a more potent murine neutralizing antibody (NAb) response on par with the spike. S2GΔHR2 elicited two-fold-higher NAb titers than the proline-capped spike (S2P), while S2GΔHR2 SApNPs derived from multilayered E2p and I3-01v9 60-mers elicited up to 10-fold higher NAb titers. The S2GΔHR2-presenting I3-01v9 SApNP also induced critically needed T-cell immunity, thereby providing a next-generation vaccine candidate to battle the COVID-19 pandemic.

ONE-SENTENCE SUMMARY (130 characters)

The receptor binding domain and stabilized SARS-CoV-2 spike were displayed on nanoparticles as vaccine antigens and elicited potent immune responses.

INTRODUCTION

Three beta-coronaviruses (β-CoVs) have caused outbreaks in humans, including the severe acute respiratory syndrome CoV-1 (SARS-CoV-1), Middle East respiratory syndrome CoV (MERS-CoV), and SARS-CoV-2, which is the causative agent of COVID-19 (*1-3*) and has resulted in more than 920,000 deaths worldwide (*4*). Enormous efforts are being undertaken to develop effective therapeutics and prophylactics for SARS-CoV-2. Small molecules that can block the host receptor, angiotensin-converting enzyme 2 (ACE2), and the transmembrane protease serine 2 (TMPRSS2) (*5*), which is required to process the spike (S) protein, are considered treatment in addition to other interventions (*6*). While the immunology underlying COVID-19 is yet to be fully understood (*6-8*), vaccine development is well underway (*9, 10*). Two inactivated vaccines have exhibited robust neutralizing antibody (NAb) responses in animals (*11, 12*), whereas vectored vaccines based on human adenovirus (Ad) type-5/26 and chimpanzee Ad (ChAdOx1) have been tested in nonhuman primates (NHPs) and human trials (*13-16*). Nucleic acid vaccines have further accelerated the response to the pandemic (*17*). Both DNA (*18-20*) and mRNA (*21*) vaccines have been rapidly developed, with moderate NAb titers observed for the mRNA vaccine in medium and high dose groups (*21*). A recombinant spike adjuvanted with lipid nanoparticles (NPs), NVX-CoV2373, was reported to elicit high NAb titers in human trials that were on average four-fold greater than in convalescent patients (*22, 23*). As of now, no vaccine has yet been approved by the U.S. Food and Drug Administration (FDA) for human use.

The SARS-CoV-2 spike protein is a trimer of S1-S2 heterodimers. The S1 subunit contains a receptor-binding domain (RBD) that binds to ACE2 on host cells to initiate infection. The S2 subunit consists of a fusion peptide (FP) and heptad repeat regions 1 and 2 (HR1 and HR2). Upon endocytosis of the virion, the S1 subunit is cleaved off to facilitate the FP insertion into the host

membrane, while the remaining S2 refolds to bring HR1 and HR2 together to fuse the viral and host cell membranes (*24*). The spike protein harbors all NAb epitopes and is the main target for vaccine development against SARS-associated CoVs (*25*). Convalescent plasma (CP) has been used to treat COVID-19 patients in severe conditions (*26*), highlighting the importance of NAbs in protection (*27*). Due to sequence conservation of RBD (but only around 73%), some previously identified NAbs targeting the SARS-CoV-1 RBD have been shown to bind and cross-neutralize SARS-CoV-2 (*28, 29*). Using single-cell technologies and SARS-CoV-2 RBD or spike as a bait, potent NAbs have now been isolated from COVID-19 patients (*30-36*). Camelid-derived single-chain NAbs have also been obtained by panning naïve or immune llama single-chain antibody (VHH) libraries (*37, 38*). Structures of SARS-CoV-2 spike and RBD in unliganded (*39, 40*), ACE2-bound (*41, 42*), and antibody-bound (*43-45*) states determined by x-ray crystallography and cryo-electron microscopy (cryo-EM) have paved the way for rational vaccine design. Cryo-EM and cryo-electron tomography (ET) have revealed the inherent spike metastability and the co-existence of pre/post-fusion spikes on virions (*46*). A double-proline mutation, S2P (*46*), has been used in most soluble constructs and all but inactivated vaccines, although a HexaPro version with greater yield and stability is now available (*47*). Cryo-ET analysis has also uncovered a dynamic, triple-hinged HR2 stalk that facilitates viral entry and immune evasion (*48-50*).

In this study, we design and optimize SARS-CoV-2 RBD/spike antigens and display them on self-assembling protein nanoparticles (SApNPs) as COVID-19 vaccine candidates. To facilitate vaccine purification, we developed an immunoaffinity column based on antibody CR3022 that binds to both SARS-CoV-1/2 RBDs (*29, 44*). We first designed a scaffolded RBD trimer to mimic the “RBD-up” spike conformation. For multivalent display, RBDs were attached to SApNPs using the SpyTag/SpyCatcher system (*51*), providing a robust and practical strategy for generating RBD

SApNP vaccines. We probed the spike metastability by comparing two uncleaved spike antigens, S2P (K986P/V987P) and S2G (K986G/V987G). The SARS-CoV-2 S2G spike exhibited abnormal behavior, suggesting that an unidentified facet of the spike can promote conformational change and block antibody access to the RBD. An HR2-deleted spike, S2GΔHR2, produced high-purity trimers, suggesting that the HR2 stalk may be a trigger of spike metastability consistent with recent findings (*48-50*). We next displayed S2GΔHR2 on ferritin (FR), E2p, and I3-01 SApNPs (*52, 53*), of which the latter two contain locking domains (LD) and helper T-cell epitopes within the protein shell (*54*). In mouse immunization, the S2P spike elicited the lowest level of NAb response. In contrast, the scaffolded RBD trimer registered two-to-three-fold higher NAb titers, with another five-fold increase in NAb titer achieved by multivalent display on FR. S2GΔHR2 elicited up to seven-fold higher NAb titers, while the two large, multilayered SApNPs induced up-to-10-fold higher NAb titers compared to S2P. Further analysis indicated that the S2GΔHR2-presenting I3-01v9 SApNP can elicit a strong Th1 response as well as other types of T-cell response needed for protective cellular immunity. Our study thus identifies the HR2 stalk as a major cause of spike metastability, validates an HR2-deleted spike design, and provides a set of RBD- and spike-based virus-like particles (VLPs) as potential effective vaccine candidates against SARS-CoV-2.

RESULTS

Rational design of scaffolded RBD trimer and RBD-presenting SApNPs

RBD binding to the ACE2 receptor initiates the membrane fusion process (*5*). The crystal structure of SARS-CoV-2 RBD/ACE2 complex revealed atomic details of receptor recognition (*55*). The SARS-CoV-2 RBD has been used as a bait to isolate monoclonal antibodies (mAbs) from patient samples (*30-36*). For SARS-CoV-1 and MERS-CoV, RBD-based vaccines have induced potent

NAbs that effectively block viral entry (*25*). Therefore, the RBD represents a major target for the humoral response during viral infection and can be used to develop epitope-focused vaccines.

We first hypothesized that RBD attached to a trimeric scaffold could mimic the "RBD-up" spike conformation and elicit NAbs that block ACE2 binding. To test this possibility, we designed a fusion construct containing SARS-CoV-1/2 RBD, a short 5-aa G_4S linker (with a 2-aa restriction site), and a trimeric viral capsid protein, SHP (PDB: 1TD0) (**Fig. 1A**). Structural modeling showed that the three tethered RBDs form a triangle of 92 Å (measured at L492), which is 14 and 18 Å wider than the SARS-CoV-1 "two-RBD-up" spike (PDB: 6CRX, measured at L478) (*56*) and the MERS-CoV "all-RBD-up" spike (PDB: 5X59, measured for L506) (*57*), respectively, allowing NAb access to each RBD. We then developed an immunoaffinity chromatography (IAC) column to facilitate tag-free purification. Previously, NAb-derived IAC columns have been used to purify HIV-1 Env trimers/NPs (*52, 53, 58, 59*), hepatitis C virus (HCV) E2 cores/NPs (*60*), and Ebola virus (EBOV) GP trimers/NPs (*54*). Tian et al. reported that a SARS-CoV-1 NAb, CR3022, can bind SARS-CoV-2 RBD (*29*). The SARS-CoV-2 RBD/CR3022 structure revealed a conserved cryptic epitope that is shared by the two SARS-CoVs, suggesting that transient breathing motions of the spike protein enable CR3022 binding to RBD (*44*). Here, we examined the utility of CR3022 in IAC columns. The SARS-CoV-1/2 RBD-5GS-1TD0 constructs were transiently expressed in 100-ml ExpiCHO cells and purified on a CR3022 column prior to size-exclusion chromatography (SEC) using a Superdex 200 10/300 GL column. While the SARS-CoV-1 RBD construct showed both aggregate (~8.6 ml) and trimer (~12.7 ml) peaks in the SEC profile, the SARS-CoV-2 RBD construct produced a single, pure trimer peak at ~12.8 ml (**Fig. 1B**). In sodium dodecyl sulfate-polyacrylamide gel electrophoresis (SDS-PAGE), a monomer band of ~37 kD and a trimer band of ~100 kD were observed under reducing and non-reducing conditions, respectively (**fig. S1A**).

Antigenicity was assessed for the two scaffolded RBD trimers in enzyme-linked immunosorbent assay (ELISA) after CR3022/SEC purification (**Fig. 1C**). RBD-specific NAbs targeting SARS-CoV-1 (CR3022 (*61*), m396 (*62*), 80R (*63*), and S230 (*64*)) and SARS-CoV-2 (B38 (*33*), CB6 (*32*), S309 from a SARS survivor (*28*), and P2B-2F6 (*31*)), were tested in ELISA. Overall, similar half maximal effective concentration (EC_{50}) values were observed for the two RBD trimers binding to their respective NAbs (**Fig. 1C**). The SARS-CoV-1 RBD trimer showed greater affinity for CR3022 than its SARS-CoV-2 counterpart with a 1.3-fold difference in the EC_{50} value, consistent with previous findings (*29, 44*). Of the SARS-CoV-2 NAbs, B38 yielded a similar EC_{50} value to CR3022. Antibody binding kinetics was measured using biolayer interferometry (BLI) (**Fig. 1D** and **fig. 1B**). Overall, all tested antibodies exhibited a fast on-rate but with visible differences in their off-rates. B38 showed a faster off-rate than other SARS-CoV-2 NAbs, while CR3022, the antibody used to purify SARS-CoV-1/2 RBD proteins, exhibited a comparable kinetic profile.

We then hypothesized that the SpyTag/SpyCatcher (or simply SPY) system can be used to conjugate RBD to SApNPs to create multivalent RBD vaccines capable of eliciting a more potent NAb response (**Fig. 1E**). The 13-aa SpyTag spontaneously reacts with the SpyCatcher protein to form an irreversible isopeptide bond (*51*). The SPY system has been successfully used to attach antigens to VLPs (*65*). Here, SpyTag was fused to the C terminus of RBD, while SpyCatcher was fused to the N terminus of an SApNP subunit, both with a 5-aa G_4S linker. This design was first tested for the 24-meric ferritin (FR) used in our previous studies (*52-54, 60*). We compared two production strategies – co-expression of RBD-5GS-SpyTag and SpyCatcher-5GS-FR versus supernatant mix after separate expression – and performed purification on a CR3022 column. Protein obtained from transient transfection in 50-ml ExpiCHO cells was analyzed by SEC on a

Superose 6 10/300 GL column (**Fig. 1F**). Both production strategies produced a peak (12 ml) corresponding to SApNPs. While the SARS-CoV-2 construct outperformed its SARS-CoV-1 counterpart in particle yield (0.6-1.0 mg versus 0.3-0.5 mg after CR3022/SEC), the supernatant mix appeared to be superior to co-expression for yield in both cases. Nonetheless, the results suggest that both strategies can be used to produce RBD SApNPs in Good Manufacturing Practice (GMP)-compatible Chinese hamster ovary (CHO) cells. Antigenicity was assessed for SEC-purified RBD-5GS-SPY-5GS-FR SApNPs. In ELISA, RBD SApNPs showed slightly improved mAb binding compared to the RBD trimers, as indicated by lower EC_{50} values (**Fig. 1G**). In BLI, a more pronounced effect of multivalent display on antigenicity was observed, showing notably increased binding signals and plateaued dissociation (**Fig. 1H** and **fig. 1C**). Structural integrity of various RBD SApNPs was analyzed by negative stain EM (nsEM) (**Figs. 1I** and **1J**). For SARS-CoV-1, an RBD-10GS-FR construct was included for comparison that produced very few SApNPs (**Fig. 1I**, left). In contrast, the RBD-5GS-SPY-5GS-FR construct produced a high yield of SApNPs with visible surface decorations (**Fig. 1I**, right). For SARS-CoV-2, the purified RBD-5GS-SPY-5GS-FR SApNPs, irrespective of the production strategy, showed morphologies corresponding to well-formed nanoparticles (**Fig. 1J**). Following a similar strategy, SARS-CoV-1/2 RBDs were also attached to a multilayered I3-01v9 SApNP (*54*) (**Fig. 1K**). Despite the modest yield (**Fig. 1L**), large SApNPs were readily observed in the EM images (**Fig. 1M**). In summary, we illustrate the utility of the SPY system for rapid development of RBD-based SApNP vaccines. Compared to the recently reported two-component RBD SApNPs (*66*), the SPY-linked RBD SApNPs presented here may be more advantageous in terms of stability and manufacturability.

Rational design of prefusion spike through minimizing metastability

In addition to the RBD, the SARS-CoV-1/2 spikes contain other NAb epitopes (*25*), which are all presented in a trimeric context (**Fig. 2A**). A double-proline mutation (2P) between HR1 and the central helix (CH) has been used to stabilize the MERS-CoV (*67*) and SARS-CoV-1 spikes (*56*). A similar 2P mutation (K986P/V987P) was introduced into the SARS-CoV-2 spike (termed S2P), which has been used to isolate and characterize NAbs (*28, 30, 35, 37-40, 43*) and is the antigen in almost all current vaccine candidates (*13-16, 18-23*). However, a recent cryo-EM study revealed an unexpected packing of S1 in the S2P spike, positioned ~12Å outwards, compared to the full-length native spike, as well as a more ordered FP proximal region (FPPR) in S2 (*46*). New designs have been generated to control the spike conformation (*68*) or to further stabilize it with more prolines (HexaPro) (*47*). Recent cryo-EM and cryo-ET studies revealed diverse spike orientations on native virions due to the highly flexible HR2 stalk (*48-50*). Previously, we identified an HR1 bend as the cause of HIV-1 Env metastability (*52, 69*) and probed the contribution of an equivalent HR1 bend and the HR2 stalk to EBOV GP metastability (*54*) to facilitate rational vaccine design. It is therefore imperative to understand SARS-CoV-2 spike metastability, and then design an optimized spike as a vaccine immunogen.

We first created His-tagged, uncleaved spike ectodomain (S_{ECTO}) constructs for SARS-CoV-1/2, both containing the 2P mutation (K986P/V987P) and a trimerization motif (1TD0) fused to the C terminus with a 5-aa G_4S linker. The two constructs were transiently expressed in 50-ml ExpiCHO cells followed by purification on either a Nickel column or a CR3022 column. The $S2P_{ECTO}$-5GS-1TD0-His_6 protein was characterized by SEC on a Superose 6 10/300 GL column (**Fig. 2B**, panels 1 and 2). After the Nickel column, both $S2P_{ECTO}$ constructs showed a trimer peak (~12 ml) with shoulders to the left and right indicative of aggregate and dimer/monomer species, respectively. CR3022 purification resulted in a consistent trimer peak and less dimer/monomer

species. We then tested a pair of S_{ECTO} constructs containing a double glycine mutation (K986G/V987G, termed 2G). The 2G mutation had little effect on the SARS-CoV-1 spike but produced abnormal SEC profiles and showed no yield for the SARS-CoV-2 spike after purification by Nickel and CR3022 columns, respectively (**Fig. 2B**, panels 3 and 4). Lastly, we tested a pair of S2G variants without the HR2 stalk (E1150-Q1208), termed S2GΔHR2. Deletion of the HR2 stalk restored the SARS-CoV-2 trimer peak and reduced aggregates for both SARS-CoVs, as shown by the SEC profiles upon CR3022 purification (**Fig. 2B**, panel 5). Since the triple-hinged HR2 stalk can generate diverse spike orientations on native virions (*48-50*), and the fusion core is formed by HR1 and HR2, we hypothesized that HR2 may be a key determinant of SARS-CoV-2 spike metastability (**Fig. 2C**, left). It is possible that the interactions between HR1 and HR2 of two neighboring spikes may facilitate the pre-to-post-fusion transition in addition to ACE2 binding and S1 dissociation. Given the extensive sequence difference in HR1 (9 amino acids in total) compared to SARS-CoV-1 (**Fig. 2C**, right), we sought to examine the role of HR1 in SARS-CoV-2 spike metastability with two HR1-swapped spike constructs. Interestingly, while HR1 swapping proved ineffective, deletion of the HR2 stalk once again restored the trimer peak (**fig. S2**, **A** to **C**). Therefore, S2GΔHR2 appeared to provide a general spike design for SARS-CoV-1/2 and perhaps other CoVs. Four separate production runs of SARS-CoV-2 S2GΔHR2-5GS-1TD0 in 300-ml ExpiCHO cells resulted in nearly identical SEC profiles with a trimer yield of 0.8-1.0 mg (**Fig. 2D**, left). Blue native polyacrylamide gel electrophoresis (BN-PAGE) confirmed the purity of the S2GΔHR2 spike across SEC fractions (**Fig. 2D**, right). Antigenicity was assessed for freshly produced SARS-CoV-2 $S2P_{ECTO}$ and S2GΔHR2 spike proteins. In ELISA, the S2GΔHR2 spike showed slightly higher affinity for the five representative mAbs than did the $S2P_{ECTO}$ spike (**Fig. 2E**). When tested against three newly identified human NAbs, C105 (*43*) and CC12.1/CC12.3

(*36*), the two spikes yielded similar EC_{50} values (**fig. S2D**). In BLI, the S2GΔHR2 spike showed higher binding signals than the $S2P_{ECTO}$ spike at the highest concentration, while exhibiting similar binding kinetics (**Fig. 2F**). The use of NAb P2B-2F6 (*31*) for spike purification resulted in higher trimer yield with similar purity to the CR3022 column across SEC fractions (**fig. S2E**). Altogether, we demonstrated that deletion of the HR2 stalk can improve spike properties and S2GΔHR2 may be a more effective spike antigen for vaccine development.

Rational design of single-component, multilayered, self-assembling spike nanoparticles

Although it was possible to conjugate trimeric SARS-CoV-2 spikes to an SApNP using the SPY system (*70*), the random, irreversible chemical linking will likely result in irregular display with unoccupied but spatially occluded anchoring sites on the surface. The SPY system is perhaps more suitable for small individual antigens, such as the RBD. Using gene fusion, we previously designed single-component SApNPs displaying stabilized HIV-1 Env trimers (*52, 53*) and optimized HCV E2 cores (*60*). Recently, we further engineered the E2p and I3-01v9 60-mers to incorporate locking domains (LDs) and helper T-cell epitopes into the constructs to create highly stable, multilayered SApNPs as multivalent carriers to develop VLP-type vaccine immunogens (*54*).

Native SARS-CoV-2 virions present both pre- and post-fusion spikes on the surface (*46, 48, 49*) (**Fig. 3A**, top). Here, our vaccine strategy aimed to develop single-component, multilayered SApNPs that each present 8 or 20 stable S2GΔHR2 spikes to the immune system (**Fig. 3A**, bottom). To explore this possibility, we modeled the S2GΔHR2 spike on ferritin (FR) with a 5-aa G_4S linker, on E2p with a 5-aa G_4S linker, and on I3-01v9 with a 10-aa $(G_4S)_2$ linker, resulting in SApNPs with diameters of 47.9 nm, 55.9 nm, and 59.3 nm, respectively (**Fig. 3B**). The three S2GΔHR2 SApNP constructs were transiently expressed in 400-ml ExpiCHO cells, followed by

CR3022 purification and SEC on a Superose 6 10/300 GL column (**Fig. 3C**). Three production runs generated highly consistent SEC profiles for all three constructs, despite the variation of low-m.w. impurities observed for the FR and E2p SApNPs. Following CR3022/SEC purification, we obtained on average 0.3-0.4 mg, 0.15-0.25 mg, and 0.3-0.35 mg SApNP for S2GΔHR2-5GS-FR, S2GΔHR2-5GS-E2p-LD4-PADRE (or E2p-L4P (*54*)), and S2GΔHR2-10GS-I3-01v9-LD7-PADRE (or I3-01v9-L7P (*54*)), respectively. Overall, S2GΔHR2-10GS-I3-01v9-L7P appeared to perform best in terms of particle yield, purity and stability in production. The structural integrity of CR3022/SEC-purified SApNPs was further characterized by nsEM, which showed well-formed particles of 45-65 nm with spikes easily recognizable on their surface (**Fig. 4D**). Antigenicity of S2GΔHR2-presenting SApNPs was assessed using the same antibody panel as above. In ELISA, three SApNPs showed slightly improved binding to some, but not all, antibodies compared to the individual spike (**Fig. 4E**). In BLI assays, we observed a clear correlation between peak antibody-binding signal and antigen valency, with E2p/I3-01v9>FR>spike (**Fig. 4F**). Multivalent display on the two 60-mers significantly improved antibody binding compared to the 24-mer. In previous studies, we observed a similar correlation for HIV-1 gp140 trimer vs. gp140 SApNPs (*52*) and HCV E2 core vs. E2 core SApNPs (*60*). In summary, these VLP-size SApNPs with 8 or 20 spikes on the surface provide promising vaccine candidates for *in vivo* evaluation.

SARS-CoV-1/2 vaccine-induced binding antibody response

Selected SARS-CoV-1/2 RBD- and spike-based immunogens were evaluated in BALB/c mice to evaluate vaccine-induced antibody responses (**Fig. 4A**). Groups of five mice were immunized four times at three-week intervals. All vaccine antigens were formulated with AddaVax, an oil-in-water emulsion adjuvant (*54*), except for I3-01v9, which was formulated with aluminum phosphate (AP) (*71*). We first performed a longitudinal analysis of binding antibody response, as measured by half

maximal effective dilution (ED_{50}), in the two SARS-CoV-2 RBD vaccine groups (**Fig. 4B** and **fig. S4**). The RBD SApNP (RBD-5GS-SPY-5GS-FR) elicited significantly higher ED_{50} titers than the scaffolded RBD trimer (RBD-5GS-1TD0) at w2 and w5, irrespective of the coating antigen, with a *P* value of 0.0009 at w8 when RBD was coated. Compared to the stabilized spike (S2GΔHR2-5GS-1TD0), the RBD SApNP elicited significantly higher ED_{50} titers against the RBD at w2, w5, and w8 (**Fig. 4B**, right), demonstrating a strong "epitope-focusing" effect. Mouse sera bound the SARS-CoV-1 spike with lower ED_{50} titers than the SARS-CoV-2 spike but with similar patterns (**fig. S4A**). We then performed a longitudinal analysis of binding antibody response induced by two SARS-CoV-2 spikes, $S2P_{ECTO}$-5GS-1TD0 and S2GΔHR2-5GS-1TD0, and three SApNPs each displaying 8 or 20 S2GΔHR2 spikes (**Fig. 4C** and **fig. S5**). The S2GΔHR2 spike elicited 2~3-fold higher average ED_{50} titers than the $S2P_{ECTO}$ spike irrespective of the coating antigen, showing greater immunogenicity (of note, to facilitate a fair comparison, mouse sera from the two spike groups were tested against their respective spikes). Three SApNPs exhibited different temporal patterns depending on the coating antigen. Using spike as the coating antigen, the I3-01v9 group showed a steady increase in average ED_{50} titer over time, with the highest average ED_{50} titers at two time pints, w2 and w8, and significantly outperforming the $S2P_{ECTO}$ spike at all time points. The I3-01v9 group also showed higher ED_{50} tiers than the S2GΔHR2 group throughout, although not with significant *P* values. The smaller FR SApNP exhibited a similar temporal pattern with lower average ED_{50} titers, but still significantly higher than the $S2P_{ECTO}$ group. Among the three SApNPs, E2p registered the lowest average ED_{50} titer at w2 and reached the highest at w5, which then decreased slightly at w8. In terms of the RBD-specific response, the five groups showed a clear ranking based on their average ED_{50} titers, which remained consistent across time points. At w2, I3-01v9 elicited an average ED_{50} titer of 175, whereas all other spike-based vaccine groups

showed little RBD-specific response. At w5 and w8, S2GΔHR2 elicited higher ED_{50} titers (on average by 2-fold) than $S2P_{ECTO}$, while all three SApNPs outperformed the individual S2GΔHR2 spike with a ranking of ED_{50} titers correlated with their size (FR<E2p<I3-01v9). Sera reacted with the SARS-CoV-1 spike similarly, albeit at a lower level (**fig. S5A**). Lastly, we compared binding antibody responses induced by three SARS-CoV-1 immunogens – $S2P_{ECTO}$ spike ($S2P_{ECTO}$-5GS-1TD0), scaffolded RBD trimer (RBD-5GS-1TD0), and RBD SApNP (RBD-5GS-SPY-5GS-FR) (**Fig. 4D** and **fig. S6**). Based on the ED_{50} values, the SARS-CoV-1 $S2P_{ECTO}$ spike appeared to be more immunogenic than the SARS-CoV-2 S2GΔHR2 spike, whereas the SARS-CoV-1 RBD SApNP was less advantageous in ED_{50} titer than its SARS-COV-2 counterpart. Serum reactivity with the SARS-CoV-2 $S2P_{ECTO}$ spike was observed for all three SARS-CoV-1 vaccine groups (**fig. S6A**). In summary, RBD SApNPs can elicit RBD-specific antibody titers at a similar or higher level compared to the spike. Furthermore, the S2GΔHR2 spike appears to be more immunogenic than the widely used $S2P_{ECTO}$ spike, in addition to its superior in-vitro properties. The multilayered E2p and I3-01v9 SApNPs are the best performers among the spike-based vaccines, consistent with our previous HIV-1, HCV, and EBOV SApNP vaccine studies (*52*, *54*, *60*).

SARS-CoV-1/2 vaccine-induced NAb response

One major goal in COVID-19 vaccine development is to generate a potent NAb response that can protect against SARS-CoV-2 infection. Pseudoparticle (SARS-CoV-1/2-pp) neutralization assays (*72*) were used to evaluate serum NAb responses elicited by different vaccine candidates. We first performed a longitudinal analysis of NAb response, as measured by half maximal inhibitory dilution (ID_{50}), in the two SARS-CoV-2 RBD vaccine groups (**Fig. 5A** and **fig. S7**). The RBD SApNP elicited a NAb response against autologous SARS-CoV-2 as early as w2, albeit with low titers, and retained its advantage at the two later time points, suggesting that such RBD SApNP

vaccines can elicit a rapid NAb response. The scaffolded RBD trimer group showed the lowest average ID_{50} titer at w5 but a NAb response comparable to that induced by the stabilized S2GΔHR2 spike at w8. A somewhat different pattern was observed in the SARS-CoV-1-pp assay. At w2, no vaccine group showed detectable heterologous NAb response. At w5 and w8, the S2GΔHR2 spike elicited a more potent SARS-CoV-1 NAb response than both RBD-based vaccines, suggesting that non-RBD epitopes may contribute to cross-neutralization. We then analyzed the NAb response induced by five spike-based vaccines longitudinally (**Fig. 5B** and **fig. S8**). In terms of autologous neutralization (**Fig. 5B**, upper panel), no spike-based vaccine elicited any SARS-CoV-2-pp NAb response at w2 after one injection. But a consistent pattern was observed for serum neutralization at w5 and w8: the $S2P_{ECTO}$ spike showed the lowest average ID_{50} titers, 879 and 2481 at w5 and w8, respectively, whereas the S2GΔHR2 spike induced a stronger NAb response with 2.8-6.7-fold higher average ID_{50} titers, which did not reach $P \leq 0.05$ due to within-group variation. Nonetheless, this result confirmed the beneficial effect of the 2P-to-2G substitution and deletion of the HR2 stalk on NAb elicitation; among the three SApNPs, E2p was the best performer at w5, showing an average ID_{50} titer of 8435 that is 9.6-fold higher than $S2P_{ECTO}$ and 1.4-fold higher than S2GΔHR2, while I3-01v9 showed the most potent NAb response at w8 with an average ID_{50} titer of 17351 that is 7-fold and 2.5-fold higher than $S2P_{ECTO}$ and S2GΔHR2, respectively. A similar temporal pattern was observed in the heterologous SARS-CoV-1-pp assay (**Fig. 5B**, lower panel). It is worth noting that the I3-01v9 SApNP elicited a SARS-CoV-1 NAb response with an average ID_{50} titer of 351 at w2, whereas all other groups showed no detectable serum neutralization. Nonetheless, these results suggest that the SARS-CoV-2 S2GΔHR2-based vaccines, particularly SApNPs, may provide protection against both SARS-CoV-1/2. Lastly, we performed a longitudinal analysis of NAb response for three SARS-CoV-1

vaccines (**Fig. 5C** and **fig. S9**). In the autologous SARS-CoV-1-pp assay, the $S2P_{ECTO}$ spike and RBD SApNP induced significantly more potent NAb responses than the scaffolded RBD trimer at w2 and w5 and all three vaccine groups showed similar ID_{50} titers at w8. However, heterologous SARS-CoV-2 neutralization was below or at the baseline level for three SARS-CoV-1 vaccines at w2, w5, and w8. The pseudovirus neutralization assay has been validated using a panel of known SARS-CoV-1/2 NAbs (**fig. S9C**). As a control, the w8 mouse sera were tested against pseudoparticles bearing the murine leukemia virus (MLV) Env, MLV-pps, and did not show non-specific neutralization (**fig. S9D**). In summary, these results demonstrate an advantage in NAb elicitation by the S2GΔHR2 spike and S2GΔHR2-presenting SApNPs compared to the $S2P_{ECTO}$ spike. Although SARS-CoV-2 RBD and S2GΔHR2 SApNPs are both effective at eliciting NAb responses that target SARS-CoV-2, S2GΔHR2 SApNPs may provide broader protection against SARS-associated CoVs.

SARS-CoV-2 vaccine-induced T-cell response

While humoral immunity is required to block host-virus interaction and prevent viral infection, cellular immunity is essential for eliminating infected host cells to control viral infection (*73-76*). Emerging evidence indicates that an early T-cell response (*77*, *78*), as well as T-cell memory (*79*), is critical for protection against SARS-CoV-2. However, COVID-19 vaccines must induce a $CD4^+$ T helper 1 (Th1), but not Th2-type, T-cell response, as the latter has been linked to vaccine-associated enhancement of respiratory disease (VAERD) (*10*). In addition, T follicular helper cells (Tfh) play an important role in the maturation and production of NAbs. Therefore, understanding T-cell responses is crucial for development of an effective and safe COVID-19 vaccine.

Interferon (IFN)-γ-producing Th1 cells are important for generating an optimal antibody response and for induction of cellular immunity (*73-75*). We first examined various SARS-CoV-2 vaccine formulations on induction of $CD4^+$ Th1 responses specific to the vaccine antigen at w11, two weeks after the fourth immunization, when memory T cells had already developed in spleen (*76*). Mouse splenocytes from the S2P group and two SApNP groups (E2p and I3-01v9) were analyzed by flow cytometry using naïve samples as a negative control. The I3-01v9 group induced about 1.5- and 2.3-fold higher frequency of IFN-γ-producing $CD4^+$ Th1 cells than the S2P and E2p groups, respectively (**Fig. 6A**). Notably, following re-stimulation with the respective antigens for as few as 4 hours, both E2p and I3-01v9 groups produced ~2-fold higher frequency of CD107a-producing cytolytic $CD4^+$ T cells than the S2P and naïve groups (**Fig. 6B**). IFN-γ/IL-4 (interleukin-4) double-positive cells are memory $CD4^+$ T cells that have acquired the ability to produce IL-4 while still retaining the ability to produce IFN-γ under Th1 conditions (*80*). It appeared that I3-01v9 induced 3- and 5-fold more IFN-γ/IL-4 double-positive memory $CD4^+$ T cells than S2P and E2p (**Fig. 6A**). These results suggest that I3-01v9 can induce both $CD4^+$ Th1 cells and IFN-γ/IL-4 double-positive memory $CD4^+$ T cells. In addition, I3-01v9 induced more IFN-γ/GM-CSF (granulocyte-macrophage colony-stimulating factor) double-positive $CD8^+$ effector T cells than S2P and E2p (**Fig. 6C**), suggesting that protective $CD8^+$ T cell responses were also generated in mice immunized with I3-01v9. Of note, $CD8^+$ T cells derived from mice immunized with I3-01v9, rather than those with S2P and E2p, acquired the ability to rapidly produce IFN-γ upon antigen re-stimulation (**Fig.6D**), suggesting generation of I3-01v9-responsive effector/memory T cells. These findings indicate that the S2GΔHR2 I3-01v9 SApNP can induce robust T-cell responses consisting of $CD4^+$ Th1 cells, IFN-γ/IL-4 double-positive memory $CD4^+$ T cells, and effector $CD8^+$ T cells, thus providing protective cellular immunity in addition to a potent NAb response. Since T cell

380 immunity against the SApNP backbone cannot be ruled out, a more detailed T-cell analysis using
381 spike antigens, SApNP backbones, and peptides for re-stimulation may be warranted.

382 **DISCUSSION**

383 COVID-19 marks the first worldwide pandemic of this scale since the infamous Spanish influenza
384 over a century ago (*81*), which caused ~50 million deaths and remains a painful reminder of our
385 vulnerability to a new virus without a protective vaccine. Therefore, the rapid spread of SARS-
386 CoV-2 demands rapid vaccine development (*10*). Operation Warp Speed (OWS) aims to deliver
387 300 million doses of safe and effective vaccines by January 2021 through a public-private
388 partnership, which has resulted in five vaccine candidates (*82*) in addition to others being tested in
389 human trials. However, vaccine development during a pandemic against a new virus poses unique
390 challenges, one of which is how to balance public health need and scientific rigor (*83-85*). The
391 global vaccine campaign also provides a unique opportunity to compare different vaccine design
392 strategies and platforms – especially new ones – against a common target.

393 Here, we approached SARS-CoV-2 vaccine development with a rational design strategy.
394 First, the choice of antigen is key to success of a vaccine irrespective of the delivery platform.
395 Most vaccine antigens including OWS's vaccine candidates are based on S2P, which produces a
396 spike structure that differs in detail from the full-length wild-type spike, e.g. in FPPR of S2 and in
397 the relative dispositions of the S1 domains (*46*). These differences may complicate interpretation
398 of vaccine outcome. S2P and other empirical spike designs (*47*) have attempted to constrain the
399 spike conformation and increase trimer yield. However, as we previously found for HIV-1 Env
400 and EBOV GP (*52, 54, 69*), it is important to identify and eliminate (if possible) the root cause of
401 spike metastability. During antigen screening, we found that deletion of the HR2 stalk with a 2P-
402 to-2G substitution renders a more stable spike, which is consistent with recent reports on a highly

flexible HR2 stalk in the native spikes on SARS-CoV-2 virions (*48-50*). Thus, S2GΔHR2 would seem to present an advance on spike design. Second, single-component SApNPs provide a new, powerful platform for VLP-type vaccine development against diverse viral pathogens (*52, 54, 60*). S2GΔHR2 was genetically fused, rather than chemically linked, to three SApNPs, including two multilayered SApNPs with enhanced stability and an embedded T-help signal. Such recombinant protein vaccines should be more effective in eliciting a potent anti-SARS-CoV-2 NAb response and less likely to induce adverse responses (*86*). An epitope-focused vaccine strategy was also explored by designing scaffolded RBD trimers and RBD-presenting SApNPs. Third, to achieve high efficacy and ensure safety, vaccine-induced NAb and T-cell responses must be evaluated in animals prior to clinical trials. Indeed, in our mouse study, the S2GΔHR2 spike appeared to be more effective than the S2P spike in NAb elicitation, both alone and displayed on SApNPs. Of note, the S2GΔHR2-presenting I3-01v9 SApNP elicited not only high NAb titers but also desired T-cell responses. In addition to viral antigen-responsive $CD4^+$ Th1 cells and memory $CD4^+$ T cells, the I3-01v9 SApNP also induced CD107a-producing cytolytic $CD4^+$ T cells, which may directly kill infected host cells, and GM-CSF-producing $CD8^+$ effector T cells, which may promote the generation of macrophages and functional dendritic cells (DCs) to facilitate the clearance of infected cells. Lastly, expression of vaccine antigens in GMP-compatible CHO cells followed by purification using an antibody column, such as CR3022, would allow rapid and industrial-scale vaccine production. In summary, our study provides promising next-generation COVID-19 vaccine candidates that are ready for evaluation in human trials.

MATERIALS AND METHODS

Design, expression and purification of SARS-CoV-2 RBD and spike antigens

The spike (S) genes of the SARS-CoV-1 isolate Tor2 (GenBank accession #: NC_004718) and the SARS-CoV-2 isolate Wuhan-Hu-1 (GenBank accession #: MN908947) were used to design all the RBD and spike constructs following codon-optimization for expression in mammalian cells. The RBD sequence is defined as P317-D518 and P330-N532 for SARS-CoV-1 and 2, respectively. The S_{ECTO} sequence is defined as M1-Q1190 and M1-Q1208 for SARS-CoV-1 and 2, respectively. To remove the S1/S2 cleavage site, an R667G mutation and a ^{682}GSAGSV^{687} modification were introduced in the SARS-CoV-1 and 2 spikes, respectively. The 2P (or 2G) mutation was made to K968/V969 and K986/V987 in the SARS-CoV-1 and 2 spikes, respectively. The SARS-CoV-2 C-terminal region (E1150-Q1208) containing the HR2 stalk was removed from $S2G_{ECTO}$, resulting in an HR2-deleted spike construct termed S2GΔHR2. The viral capsid protein SHP (PDB: 1TD0) was used as a trimerization motif in spike constructs for immunization, whereas the foldon domain from the bacteriophage T4 fibritin (PDB: 1RFO) was used in coating spike antigens for ELISA to mask the 1TD0-derived antibody response. All constructs were transiently expressed in ExpiCHO cells (Thermo Fisher). Briefly, ExpiCHO cells were thawed and incubated with ExpiCHO™ Expression Medium (Thermo Fisher) in a shaker incubator at 37 °C, 135 rpm and 8% CO_2. When the cells reached a density of 10×10^6 ml^{-1}, ExpiCHO™ Expression Medium was added to reduce cell density to 6×10^6 ml^{-1} for transfection. The ExpiFectamine™ CHO/plasmid DNA complexes were prepared for 100-ml transfection in ExpiCHO cells following the manufacturer's instructions. For a given construct, 100 μg of plasmid and 320 μl of ExpiFectamine™ CHO reagent were mixed in 7.7 ml of cold OptiPRO™ medium (Thermo Fisher). After the first feed on day one, ExpiCHO cells were cultured in a shaker incubator at 33 °C, 115 rpm and 8% CO_2 following the Max Titer protocol with an additional feed on day five (Thermo Fisher). Culture supernatants were harvested 13 to 14 days after transfection, clarified by centrifugation at 4000 rpm for 25 min, and filtered

using a 0.45 μm filter (Thermo Fisher). The CR3022 antibody column was used to extract SARS-CoV-1/2 antigens from the supernatants, which was followed by SEC on a Superdex 200 10/300 GL column (for scaffolded RBD trimer) or a Superose 6 10/300 GL column (for RBD-SPY-SApNPs, spikes, and spike-presenting SApNPs). For comparison, His-tagged S_{ECTO}-5GS-1TD0 spike protein was extracted from the supernatants using an immobilized Ni Sepharose™ Excel column (GE Healthcare) and eluted with 500 mM Imidazole prior to SEC. Protein concentration was determined using UV_{280} absorbance with theoretical extinction coefficients.

Blue native polyacrylamide gel electrophoresis

SARS-CoV-2 spikes and spike-presenting SApNPs were analyzed by blue native polyacrylamide gel electrophoresis (*BN-PAGE*) and stained with Coomassie blue. The proteins were mixed with sample buffer and G250 loading dye and added to a 4-12% Bis-Tris NativePAGE™ gel (Life Technologies). BN-PAGE gels were run for 2 to 2.5 hours at 150 V using the NativePAGE™ running buffer (Life Technologies) according to the manufacturer's instructions.

Enzyme-linked immunosorbent assay

Each well of a Costar™ 96-well assay plate (Corning) was first coated with 50 μl PBS containing 0.2 μg of the appropriate antigens. The plates were incubated overnight at 4 °C, and then washed five times with wash buffer containing PBS and 0.05% (v/v) Tween 20. Each well was then coated with 150 μl of a blocking buffer consisting of PBS, 40 mg ml^{-1} blotting-grade blocker (Bio-Rad), and 5% (v/v) FBS. The plates were incubated with the blocking buffer for 1 hour at room temperature, and then washed five times with wash buffer. For antigen binding, antibodies were diluted in the blocking buffer to a maximum concentration of 5 μg ml^{-1} followed by a 10-fold

dilution series. For each antibody dilution, a total of 50 μl volume was added to the appropriate wells. For mouse sample analysis, serum or plasma was diluted by 20-fold in the blocking buffer and subjected to a 10-fold dilution series. For each sample dilution, a total of 50 μl volume was added to the wells. Each plate was incubated for 1 hour at room temperature, and then washed 5 times with PBS containing 0.05% Tween 20. For antibody binding, a 1:5000 dilution of goat anti-human IgG antibody (Jackson ImmunoResearch Laboratories, Inc), or for mouse sample analysis, a 1:3000 dilution of horseradish peroxidase (HRP)-labeled goat anti-mouse IgG antibody (Jackson ImmunoResearch Laboratories), was then made in the wash buffer (PBS containing 0.05% Tween 20), with 50 μl of this diluted secondary antibody added to each well. The plates were incubated with the secondary antibody for 1 hour at room temperature, and then washed 5 times with PBS containing 0.05% Tween 20. Finally, the wells were developed with 50 μl of TMB (Life Sciences) for 3-5 min before stopping the reaction with 50 μl of 2 N sulfuric acid. The resulting plate readouts were measured at a wavelength of 450 nm. Of note, the w2 serum binding did not reach the plateau (or saturation) to allow for accurate determination of ED_{50} titers. Nonetheless, the ED_{50} values at w2 were derived by setting the lower/upper constraints of OD_{450} at 0.0/3.2 to facilitate the comparison of different vaccine groups at the first time point.

Bio-layer interferometry

The kinetics of SARS-CoV-1/2 vaccine antigens, RBD versus RBD-presenting SApNPs as well as spike versus spike-presenting SApNPs, binding to a panel of known antibodies was measured using an Octet RED96 instrument (FortéBio, Pall Life Sciences). All assays were performed with agitation set to 1000 rpm in FortéBio 1× kinetic buffer. The final volume for all the solutions was 200 μl per well. Assays were performed at 30 °C in solid black 96-well plates (Geiger Bio-One).

For all antigens with the exception of S2GΔHR2-NPs, 5 μg ml^{-1} of antibody in 1× kinetic buffer was loaded onto the surface of anti-human Fc Capture Biosensors (AHC) for 300 s. For S2GΔHR2-NPs, anti-human Fc Quantitation Biosensors (AHQ) were used. A 60 s biosensor baseline step was applied prior to the analysis of the association of the antibody on the biosensor to the antigen in solution for 200 s. A two-fold concentration gradient of antigen, starting at 950 nM for scaffolded RBD trimers, 37 nM for RBD-5GS-SPY-5GS-FR SApNP, 150 nM for spike trimers, and 9/3.5/3.5 nM for S2GΔHR2 presented on FR/E2p/I3-01v9 SApNPs, was used in a titration series of six. The dissociation of the interaction was followed for 300 s. Correction of baseline drift was performed by subtracting the mean value of shifts recorded for a sensor loaded with antibody but not incubated with antigen and for a sensor without antibody but incubated with antigen. Octet data were processed by FortéBio's data acquisition software v.8.1. Experimental data were fitted with the binding equations describing a 2:1 interaction to achieve optimal fitting. Of note, S2GΔHR2 trimer binding was also measured using AHQ to facilitate the comparison of antibody binding with S2GΔHR2-presenting SApNPs.

Electron microscopy (EM) assessment of nanoparticle constructs

The initial EM analysis of RBD and S2GΔHR2-presenting SApNPs was conducted at the Core Microscopy Facility at The Scripps Research Institute. Briefly, SApNP samples were prepared at the concentration of 0.01 mg/ml. Carbon-coated copper grids (400 mesh) were glow-discharged and 8 μL of each sample was adsorbed for 2 min. Excess sample was wicked away and grids were negatively stained with 2% uranyl formate for 2 min. Excess stain was wicked away and the grids were allowed to dry. Samples were analyzed at 80 kV with a Talos L120C transmission electron microscope (Thermo Fisher) and images were acquired with a CETA 16M CMOS camera.

517

518 **Animal immunization and sample collection**

519 Similar immunization protocols have been reported in our previous SApNP vaccine studies.
520 Briefly, the Institutional Animal Care and Use Committee (IACUC) guidelines were followed with
521 animal subjects tested in the immunization study. Eight-week-old BALB/c mice were purchased
522 from The Jackson Laboratory and housed in ventilated cages in environmentally controlled rooms
523 at The Scripps Research Institute, in compliance with an approved IACUC protocol and AAALAC
524 (Association for Assessment and Accreditation of Laboratory Animal Care) International
525 guidelines. Mice were immunized at weeks 0, 3, 6, and 9 with 200 µl of antigen/adjuvant mix
526 containing 50 µg of vaccine antigen and 100 µl of adjuvant, AddaVax or Adju-Phos (InvivoGen),
527 via the intraperitoneal (i.p.) route. Blood was collected two weeks after each immunization. All
528 bleeds were performed through the retro-orbital sinus using heparinized capillary tubes into
529 EDTA-coated tubes. Samples were diluted with an equal volume of PBS and then overlaid on 4.5
530 ml of Ficoll in a 15 ml SepMate^{TM} tube (STEMCELL Technologies) and spun at 1200 RPM for
531 10 min at 20 °C to separate plasma and cells. The plasma was heat inactivated at 56 °C for 30 min,
532 spun at 1200 RPM for 10 min, and sterile filtered. The cells were washed once in PBS and then
533 resuspended in 1 ml of ACK Red Blood Cell lysis buffer (Lonza). After washing with PBS,
534 peripheral blood mononuclear cells (PBMCs) were resuspended in 2 ml of Bambanker Freezing
535 Media (Lymphotec). Spleens were also harvested and ground against a 70-µm cell strainer (BD
536 Falcon) to release the splenocytes into a cell suspension. Splenocytes were centrifuged, washed in
537 PBS, treated with 5 ml of ACK lysing buffer (Lonza), and frozen with 3ml of Bambanker freezing
538 media. Sera were heat inactivated for ELISA binding and pseudovirus neutralization assays.

539 **SARS-CoV-1/2 pseudovirus neutralization assay**

Pseudoparticle (SARS-CoV-1/2-pp) neutralization assays were utilized to assess the neutralizing activity of previously reported antibodies and vaccine-induced murine antibody response. SARS-CoV-1/2-pps were generated by co-transfection of HEK293T cells with the HIV-1 pNL4-3.lucR-E- plasmid (obtained from the NIH AIDS reagent program: https://www.aidsreagent.org/) and the expression plasmid encoding the S gene of SARS-CoV-1 isolate Tor2 (GenBank accession #: NC_004718) and the SARS-CoV-2 isolate Wuhan-Hu-1 (GenBank accession #: MN908947) at a 4:1 ratio by lipofectamine 3000 (Thermo Fisher Scientific). After 48 to 72 hours, SARS-CoV-1/2-pps were collected from the supernatant by centrifugation at 4000 rpm for 10 min, aliquoted, and stored at -80 °C before use. The mAbs at a starting concentration of 0.1-10 μg/ml, or mouse serum at a starting dilution of 100-fold, were mixed with the supernatant containing SARS-CoV-1/2-pps and incubated for 1 hour at 37°C in white solid-bottom 96-well plate (Corning). A 3-fold dilution series was used in the assay. The HEK293T-hACE2 cell line (catalogue#: NR-52511) and the vector pcDNA3.1(-) containing the SARS-CoV-2 S gene (catalogue#: NR52420) were obtained from BEI RESOURCES (https://www.beiresources.org/) and used in pseudovirus neutralization assays (*72*). Briefly, HEK293T-hACE2 cells at 1×10^4 were added to each well and the plate was incubated at 37°C for 48 hours. After incubation, overlying media was removed, and cells were lysed. The firefly luciferase signal from infected cells was determined using the Bright-Glo Luciferase Assay System (Promega) according to the manufacturer's instructions. Data were retrieved from a BioTek microplate reader with Gen 5 software, the average background luminescence from a series of uninfected wells was subtracted from each well, and neutralization curves were generated using GraphPad Prism 8.4.3, in which values from wells were compared against a well containing SARS-CoV-1/2-pp only. Due to the difference in mouse samples (serum: Pre, w2, w5, and w8; plasma: w11) and the sensitivity of SARS-CoV-2-pp assays, the w11 NAb

563 responses were not compared but included in figs. S7-S9 for the sake of completeness. The same
564 HIV-1 vectors pseudotyped with the murine leukemia virus (MLV) Env gene, termed MLV-pps,
565 were produced in HEK293T cells and included in the neutralization assays as a negative control.

566 **Dendritic cell (DC) production**

567 Mouse bone marrow (BM) was cultured in RPMI 1640 medium containing 10% fetal bovine serum
568 and recombinant mouse Flt3L (50 ng/mL) and SCF (10 ng/ml) for 9 days as described (*87*). To
569 induce DC activation, immature DCs were incubated with lipopolysaccharide (LPS, 100 ng/mL),
570 R848 (Resiquimod, 100 ng/mL) or CpG (ODN 1585, 1μM) overnight, which activated Toll-like
571 receptor (TLR)4 , TLR7/8 or TLR9 signaling, respectively. Cells were harvested for experiments.
572 pDCs were sorted to isolate CD11c+B220+ cells using FACS cell sorter and magnetic beads
573 (Miltenyi-Biotech, CA).

574 **Antibodies and flow cytometry analysis**

575 All antibodies used for immunofluorescence staining were purchased from eBioscience (San
576 Diego, CA), BioLegend (San Diego, CA) or BD Biosciences (San Jose, CA). Magnetic microbead-
577 conjugated Abs and streptavidin were purchased from Miltenyi-Biotech (Auburn, CA).
578 Recombinant human IL-2 protein was purchased from R&D Systems (Minneapolis, MN).
579 Recombinant mouse Flt3 ligand (Flt3L) and mouse SCF were purchased from Shenandoah Biotech
580 (Warwick, PA). Cells were stained with appropriate concentrations of mAbs. Dead cells were
581 excluded using Fixable Viability Dye from eBioscience (San Diego, CA). Flow cytometry (FC)
582 analyses were performed using LSRII (BD Bioscience, CA) and Canto cytometers (Becton
583 Dickinson, NJ). Cells were sorted on BD FACSAria II (BD Bioscience, CA).

584 **T cell culture and activation**

Splenic mononuclear cells from each group of immunized mice were cultured in the presence of DCs pulsed with or without S2P, E2P or I3-01v9 SApNP (1×10^{-7} μM) in complete IMDM medium containing IL-2 (5.0 ng/ml). Cells were collected 16 hours and 4 hours later for intracellular cytokine staining and flow cytometric analysis.

Statistics

In antibody analysis, comparison of different vaccine groups was performed in GraphPad Prism 8.4.3 using the two-tailed unpaired Student's *t* test. In T cell analysis, comparison of means was done using the two-tailed unpaired Student's t test, ANOVA and then post-hoc *t* test. P values of 0.05 or less were considered significant.

SUPPLEMENTARY MATERIALS

Supplementary material for this article is available at http://xxx/xxx/xxx.

fig. S1. In-vitro characterization of SARS-CoV-1/2 RBD-based immunogens.

fig. S2. In-vitro characterization of SARS-CoV-2 spikes.

fig. S3. In-vitro characterization of SARS-CoV-2 S2GΔHR2 SApNPs.

fig. S4. SARS-CoV-2 RBD/RBD-SApNP vaccine-induced binding antibody response.

fig. S5. SARS-CoV-2 spike/spike-SApNP vaccine-induced binding antibody response.

fig. S6. Design and characterization of multilayered EBOV GPΔmuc-presenting SApNPs.

fig. S7. SARS-CoV-2 RBD/RBD-SApNP vaccine-induced neutralizing antibody response.

fig. S8. SARS-CoV-2 spike/spike-SApNP vaccine-induced neutralizing antibody response.

fig. S9. SARS-CoV-1 spike/RBD/RBD-SApNP vaccine-induced neutralizing antibody response.

fig. S10. T-cell response induced by $S2P_{ECTO}$ and S2GΔHR2-presenting SApNPs.

References

1. N. Zhu *et al.*, A Novel Coronavirus from Patients with Pneumonia in China, 2019. *N. Engl. J. Med.* **382**, 727-733 (2020).
2. P. Zhou *et al.*, A pneumonia outbreak associated with a new coronavirus of probable bat origin. *Nature* **579**, 270-273 (2020).
3. F. Wu *et al.*, A new coronavirus associated with human respiratory disease in China. *Nature* **579**, 265-226 (2020).
4. E. S. Dong, H. R. Du, L. Gardner, An interactive web-based dashboard to track COVID-19 in real time. *Lancet Infect. Dis.* **20**, 533-534 (2020).
5. M. Hoffmann *et al.*, SARS-CoV-2 cell entry depends on ACE2 and TMPRSS2 and is blocked by a clinically proven protease inhibitor. *Cell* **181**, 271-280.e278 (2020).
6. M. Z. Tay, C. M. Poh, L. Renia, P. A. MacAry, L. F. P. Ng, The trinity of COVID-19: immunity, inflammation and intervention. *Nat. Rev. Immunol.* **20**, 363-374 (2020).
7. T. Zohar, G. Alter, Dissecting antibody-mediated protection against SARS-CoV-2. *Nat. Rev. Immunol.* **20**, 392-394 (2020).
8. N. Vabret *et al.*, Immunology of COVID-19: Current State of the Science. *Immunity* **52**, 910-941 (2020).
9. N. Lurie, M. Saville, R. Hatchett, J. Halton, Developing Covid-19 Vaccines at Pandemic Speed. *N. Engl. J. Med.* **382**, 1969-1973 (2020).
10. B. S. Graham, Rapid COVID-19 vaccine development. *Science* **368**, 945-946 (2020).
11. Q. Gao *et al.*, Development of an inactivated vaccine candidate for SARS-CoV-2. *Science* **369**, 77-81 (2020).
12. H. Wang *et al.*, Development of an inactivated vaccine candidate, BBIBP-CorV, with potent protection against SARS-CoV-2. *Cell* **182**, 713-721.e719 (2020).
13. N. van Doremalen *et al.*, ChAdOx1 nCoV-19 vaccine prevents SARS-CoV-2 pneumonia in rhesus macaques. *Nature*, Online ahead of print (2020).
14. P. M. Folegatti *et al.*, Safety and immunogenicity of the ChAdOx1 nCoV-19 vaccine against SARS-CoV-2: a preliminary report of a phase 1/2, single-blind, randomised controlled trial. *Lancet* **396**, 467-478 (2020).
15. N. B. Mercado *et al.*, Single-shot Ad26 vaccine protects against SARS-CoV-2 in rhesus macaques. *Nature*, Online ahead of print (2020).
16. F.-C. Zhu *et al.*, Safety, tolerability, and immunogenicity of a recombinant adenovirus type-5 vectored COVID-19 vaccine: a dose-escalation, open-label, non-randomised, first-in-human trial. *Lancet* **395**, 1845-1854 (2020).
17. E. N. Gary, D. B. Weiner, DNA vaccines: prime time is now. *Curr. Opin. Immunol.* **65**, 21-27 (2020).
18. T. R. F. Smith *et al.*, Immunogenicity of a DNA vaccine candidate for COVID-19. *Nat. Commun.* **11**, 2601 (2020).
19. J. Yu *et al.*, DNA vaccine protection against SARS-CoV-2 in rhesus macaques. *Science* **369**, 806-811 (2020).
20. A. Patel *et al.*, Intradermal-delivered DNA vaccine provides anamnestic protection in a rhesus macaque SARS-CoV-2 challenge model. *bioRxiv*, 2020.2007.2028.225649 (2020).
21. L. A. Jackson *et al.*, An mRNA Vaccine against SARS-CoV-2 - Preliminary Report. *N. Engl. J. Med.*, Online ahead of print (2020).

22. C. Keech *et al.*, First-in-Human Trial of a SARS CoV 2 Recombinant Spike Protein Nanoparticle Vaccine. *medRxiv*, 2020.2008.2005.20168435 (2020).
23. J.-H. Tian *et al.*, SARS-CoV-2 spike glycoprotein vaccine candidate NVX-CoV2373 elicits immunogenicity in baboons and protection in mice. *bioRxiv*, 2020.2006.2029.178509 (2020).
24. J. Shang *et al.*, Cell entry mechanisms of SARS-CoV-2. *Proc. Natl. Acad. Sci. U. S. A.* **117**, 11727-11734 (2020).
25. L. Y. Du *et al.*, The spike protein of SARS-CoV - a target for vaccine and therapeutic development. *Nat. Rev. Microbiol.* **7**, 226-236 (2009).
26. K. Duan *et al.*, Effectiveness of convalescent plasma therapy in severe COVID-19 patients. *Proc. Natl. Acad. Sci. U. S. A.* **117**, 9490-9496 (2020).
27. S. B. Jiang, C. Hillyer, L. Y. Du, Neutralizing antibodies against SARS-CoV-2 and other human coronaviruses. *Trends Immunol.* **41**, 355-359 (2020).
28. D. Pinto *et al.*, Cross-neutralization of SARS-CoV-2 by a human monoclonal SARS-CoV antibody. *Nature* **583**, 290-295.
29. X. Tian *et al.*, Potent binding of 2019 novel coronavirus spike protein by a SARS coronavirus-specific human monoclonal antibody. *Emerg. Microbes Infect.* **9**, 382-385 (2020).
30. S. J. Zost *et al.*, Rapid isolation and profiling of a diverse panel of human monoclonal antibodies targeting the SARS-CoV-2 spike protein. *Nat. Med.*, Online ahead of print.
31. B. Ju *et al.*, Human neutralizing antibodies elicited by SARS-CoV-2 infection. *Nature* **584**, 115-119 (2020).
32. R. Shi *et al.*, A human neutralizing antibody targets the receptor-binding site of SARS-CoV-2. *Nature* **584**, 120-124 (2020).
33. Y. Wu *et al.*, A noncompeting pair of human neutralizing antibodies block COVID-19 virus binding to its receptor ACE2. *Science* **368**, 1274-1278 (2020).
34. Y. L. Cao *et al.*, Potent Neutralizing Antibodies against SARS-CoV-2 Identified by High-Throughput Single-Cell Sequencing of Convalescent Patients' B Cells. *Cell* **182**, 73-84.e16 (2020).
35. D. F. Robbiani *et al.*, Convergent antibody responses to SARS-CoV-2 in convalescent individuals. *Nature* **584**, 437-442 (2020).
36. T. F. Rogers *et al.*, Isolation of potent SARS-CoV-2 neutralizing antibodies and protection from disease in a small animal model. *Science* **369**, 956-963 (2020).
37. J. D. Huo *et al.*, Neutralizing nanobodies bind SARS-CoV-2 spike RBD and block interaction with ACE2. *Nat. Struct. Mol. Biol.*, Online ahead of print.
38. D. Wrapp *et al.*, Structural basis for potent neutralization of betacoronaviruses by single-domain camelid antibodies. *Cell* **181**, 1004-1015.e1015 (2020).
39. D. Wrapp *et al.*, Cryo-EM structure of the 2019-nCoV spike in the prefusion conformation. *Science* **367**, 1260-1263 (2020).
40. A. C. Walls *et al.*, Structure, Function, and Antigenicity of the SARS-CoV-2 Spike Glycoprotein. *Cell* **181**, 281-292.e286 (2020).
41. R. Yan *et al.*, Structural basis for the recognition of SARS-CoV-2 by full-length human ACE2. *Science* **367**, 1444-1448 (2020).
42. J. Shang *et al.*, Structural basis of receptor recognition by SARS-CoV-2. *Nature* **581**, 221-224 (2020).

43. C. O. Barnes *et al.*, Structures of human antibodies bound to SARS-CoV-2 spike reveal common epitopes and recurrent features of antibodies. *Cell* **82**, 828-842.e816 (2020).
44. M. Yuan *et al.*, A highly conserved cryptic epitope in the receptor binding domains of SARS-CoV-2 and SARS-CoV. *Science* **368**, 630-633 (2020).
45. M. Yuan *et al.*, Structural basis of a shared antibody response to SARS-CoV-2. *Science* **369**, 1119-1123 (2020).
46. Y. Cai *et al.*, Distinct conformational states of SARS-CoV-2 spike protein. *Science*, Online ahead of print (2020).
47. C.-L. Hsieh *et al.*, Structure-based design of prefusion-stabilized SARS-CoV-2 spikes. *Science*, Online ahead of print (2020).
48. H. Yao *et al.*, Molecular architecture of the SARS-CoV-2 virus. *bioRxiv*, 2020.2007.2008.192104 (2020).
49. Z. Ke *et al.*, Structures and distributions of SARS-CoV-2 spike proteins on intact virions. *Nature*, Online ahead of print (2020).
50. B. Turonova *et al.*, In situ structural analysis of SARS-CoV-2 spike reveals flexibility mediated by three hinges. *Science*, Online ahead of print (2020).
51. B. Zakeri *et al.*, Peptide tag forming a rapid covalent bond to a protein, through engineering a bacterial adhesin. *Proc. Natl. Acad. Sci. U. S. A.* **109**, E690-E697 (2012).
52. L. He *et al.*, HIV-1 vaccine design through minimizing envelope metastability. *Sci. Adv.* **4**, aau6769 (2018).
53. L. He *et al.*, Presenting native-like trimeric HIV-1 antigens with self-assembling nanoparticles. *Nat. Commun.* **7**, 12041 (2016).
54. L. He *et al.*, Single-component multilayered self-assembling nanoparticles presenting rationally designed glycoprotein trimers as Ebola virus vaccines. *bioRxiv*, 2020.2008.2022.262634 (2020).
55. J. Lan *et al.*, Structure of the SARS-CoV-2 spike receptor-binding domain bound to the ACE2 receptor. *Nature* **581**, 215-220 (2020).
56. R. N. Kirchdoerfer *et al.*, Stabilized coronavirus spikes are resistant to conformational changes induced by receptor recognition or proteolysis. *Sci. Rep.* **8**, 15701 (2018).
57. Y. Yuan *et al.*, Cryo-EM structures of MERS-CoV and SARS-CoV spike glycoproteins reveal the dynamic receptor binding domains. *Nat. Commun.* **8**, 15092 (2017).
58. R. W. Sanders *et al.*, A next-generation cleaved, soluble HIV-1 Env trimer, BG505 SOSIP.664 gp140, expresses multiple epitopes for broadly neutralizing but not non-neutralizing antibodies. *PLoS Pathog.* **9**, e1003618 (2013).
59. P. Pugach *et al.*, A native-like SOSIP.664 trimer based on an HIV-1 subtype B env gene. *J. Virol.* **89**, 3380-3395 (2015).
60. L. L. He *et al.*, Proof of concept for rational design of hepatitis C virus E2 core nanoparticle vaccines. *Sci. Adv.* **6**, eaaz6225 (2020).
61. J. ter Meulen *et al.*, Human monoclonal antibody combination against SARS coronavirus: Synergy and coverage of escape mutants. *PLoS Med.* **3**, 1071-1079 (2006).
62. P. Prabakaran *et al.*, Structure of severe acute respiratory syndrome coronavirus receptor-binding domain complexed with neutralizing antibody. *J. Biol. Chem.* **281**, 15829-15836 (2006).
63. W. C. Hwang *et al.*, Structural basis of neutralization by a human anti-severe acute respiratory syndrome spike protein antibody, 80R. *J. Biol. Chem.* **281**, 34610-34616 (2006).

64. A. C. Walls *et al.*, Unexpected receptor functional mimicry elucidates activation of coronavirus fusion. *Cell* **176**, 1026-1039.e1015 (2019).
65. T. U. J. Bruun, A. M. C. Andersson, S. J. Draper, M. Howarth, Engineering a rugged nanoscaffold to enhance plug-and-display vaccination. *Acs Nano* **12**, 8855-8866 (2018).
66. A. C. Walls *et al.*, Elicitation of potent neutralizing antibody responses by designed protein nanoparticle vaccines for SARS-CoV-2. *bioRxiv*, 2020.2008.2011.247395 (2020).
67. J. Pallesen *et al.*, Immunogenicity and structures of a rationally designed prefusion MERS-CoV spike antigen. *Proc. Natl. Acad. Sci. U. S. A.* **114**, E7348-E7357 (2017).
68. R. Henderson *et al.*, Controlling the SARS-CoV-2 spike glycoprotein conformation. *Nat. Struct. Mol. Biol.*, Online ahead of print (2020).
69. L. Kong *et al.*, Uncleaved prefusion-optimized gp140 trimers derived from analysis of HIV-1 envelope metastability. *Nat. Commun.* **7**, 12040 (2016).
70. B. Zhang *et al.*, A versatile platform to incorporate viral trimeric antigens into self-assembling nanoparticle immunogens. *bioRxiv*, 2020.2006.2011.147496 (2020).
71. P. J. Hotez, D. B. Corry, U. Strych, M. E. Bottazzi, COVID-19 vaccines: neutralizing antibodies and the alum advantage. *Nat. Rev. Immunol.*, (2020).
72. K. H. D. Crawford *et al.*, Protocol and reagents for pseudotyping lentiviral particles with SARS-CoV-2 spike protein for neutralization assays. *Viruses* **12**, 513 (2020).
73. E. S. Rosenberg *et al.*, Vigorous HIV-1-specific CD4(+) T cell responses associated with control of viremia. *Science* **278**, 1447-1450 (1997).
74. L. M. Snell *et al.*, Overcoming CD4 Th1 cell fate restrictions to sustain antiviral CD8 T cells and control persistent virus infection. *Cell Rep.* **16**, 3286-3296 (2016).
75. J. F. Zhu, H. Yamane, W. E. Paul, Differentiation of effector CD4 T cell populations. *Annu. Rev. Immunol.* **28**, 445-489 (2010).
76. B. J. Laidlaw, J. E. Craft, S. M. Kaech, The multifaceted role of CD4(+) T cells in CD8(+) T cell memory. *Nat. Rev. Immunol.* **16**, 102-111 (2016).
77. A. Grifoni *et al.*, Targets of T cell responses to SARS-CoV-2 coronavirus in humans with COVID-19 disease and unexposed individuals. *Cell* **181**, 1489-1501.e1415 (2020).
78. M. Jeyanathan *et al.*, Immunological considerations for COVID-19 vaccine strategies *Nat. Rev. Immunol.*, Online ahead of print (2020).
79. Y. Peng *et al.*, Broad and strong memory CD4+ and CD8+ T cells induced by SARS-CoV-2 in UK convalescent COVID-19 patients. *bioRxiv*, 2020.2006.2005.134551 (2020).
80. C. M. Krawczyk, H. Shen, E. J. Pearce, Functional plasticity in memory T helper cell responses. *J. Immunol.* **178**, 4080-4088 (2007).
81. J. K. Taubenberger, D. M. Morens, 1918 influenza: the mother of all pandemics. *Emerg. Infect. Dis.* **12**, 15-22 (2006).
82. K. P. O'Callaghan, A. M. Blatz, P. A. Offit, Developing a SARS-CoV-2 vaccine at warp speed. *J. Am. Med. Assoc.* **324**, 437-438 (2020).
83. G. A. Poland, Tortoises, hares, and vaccines: A cautionary note for SARS-CoV-2 vaccine development. *Vaccine* **38**, 4219-4220 (2020).
84. L. Corey, J. R. Mascola, A. S. Fauci, F. S. Collins, A strategic approach to COVID-19 vaccine R&D. *Science* **368**, 948-950 (2020).
85. M. S. Diamond, T. C. Pierson, The challenges of vaccine development against a new virus during a pandemic. *Cell Host Microbe* **27**, 699-703 (2020).
86. J. P. Moore, P. J. Klasse, COVID-19 vaccines: "warp speed" needs mind melds, not warped minds. *J. Virol.* **94**, e01083-01020 (2020).

87. K. Mochizuki *et al.*, Programming of donor T cells using allogeneic delta-like ligand 4-positive dendritic cells to reduce GVHD in mice. *Blood* **127**, 3270-3280 (2016).

Acknowledgements: Funding: This work was funded by NIH Grants AI129698 and AI140844 (to J.Z.), Ufovax/SFP-2018-0416, Ufovax/SFP-2018-1013 and Ufovax/SFP-2020-0111 (to J.Z.).

Author contributions: Project design by L.H., Y.Z., I.A.W. and J.Z; construct design of RBD and spike-based immungoens by L.H. and J.Z.; plasmid design and processing by L.H. and C.S.; antigen production, purification and basic characterization by L.H., X.L., and T.N.; antibody production and column packing by L.H., X.L., and T.N.; antibody-antigen ELISA and BLI by L.H. and C.S.; serum-antigen ELISA by L.H., X.L., and C.S.; antibody and mouse serum neutralization by L.H. and X.L.; vaccine-induced T-cell response analysis by Y.W., C.A., and Y.Z.; Manuscript written by L.H., Y.Z., I.A.W. and J.Z. All authors were asked to comment on the manuscript. The TSRI manuscript number is 30028. **Competing interests:** Authors declare no competing interests. **Data and materials availability:** All data are available in the main text or in the supplementary materials. Additional data related to this paper may be requested from the corresponding author.

Figure legends

Fig. 1. Rational design of SARS-CoV-1/2 RBD-based vaccines. (A) Structural model of RBD-5GS-1TD0 in an extended RBD-up conformation. 1TD0 is a trimerization scaffold of viral origin. Left: top view; Right: side view. **(B)** SEC profiles of SARS-CoV-1/2 scaffolded RBD trimers following ExpiCHO expression and CR3022 purification. **(C)** ELISA binding of SARS-CoV-1/2 scaffolded RBD trimers to a panel of mAbs/NAbs. EC_{50} (μg/ml) values are labeled on the plot. **(D)** Octet binding of the SARS-CoV-2 scaffolded RBD trimer to five mAbs/NAbs. Sensorgrams were obtained from an Octet RED96 instrument at six antigen concentrations from 950 to 29.5nM by twofold dilution. **(E)** Diagram of conjugating RBD to the 24-meric FR SApNP using the

SpyTag/SpyCatcher (SPY) system. **(F)** SEC profiles of SARS-CoV-1/2 RBD-5GS-SPY-5GS-FR SApNPs produced by co-expression (black line) and supernatant mix (red line). **(G)** ELISA binding of SARS-CoV-1/2 RBD-FR SApNPs to a panel of mAbs/NAbs. EC_{50} (μg/ml) values are labeled on the plot. **(H)** Octet binding of the SARS-CoV-2 RBD-FR SApNP to five mAbs/NAbs. Sensorgrams were obtained from an Octet RED96 instrument at six antigen concentrations from 37 to 1.1nM by twofold dilution. **(I)** EM images of SARS-CoV-1 RBD-10GS-FR (left) and RBD-5GS-SPY-5GS-FR (right). **(J)** EM images of SARS-CoV-2 RBD-5GS-SPY-5GS-FR obtained from co-expression (left) and supernatant mix (right). **(K)** Diagram of conjugating RBD to the 60-meric multilayered I3-01v9 SApNP using the SPY system. **(L)** and **(M)** SEC profiles and EM images of SARS-CoV-1/2 RBD-5GS-SPY-5GS-I3-01v9-LD7-PADRE (or -L7P) SApNPs.

Fig. 2 Rational design of SARS-CoV-2 spike antigens. (A) Structural model of prefusion S spike linked to the C-terminal trimerization domain (1TD0) with a 5GS linker in transparent molecular surface. The approximate position for the unstructured HR2 stalk, or in this case a 5-aa G_4S linker, is highlighted with a dashed line box. **(B)** SEC profiles of SARS-CoV-1 spikes (top) and SARS-CoV-2 spikes (bottom). From left to right: the $S2P_{ECTO}$-5GS-1TD0 spike purified on a Nickel column (panel 1) and on a CR3022 column (panel 2), the $S2G_{ECTO}$-5GS-1TD0 spike purified on a Nickel column (panel 3) and CR3022 column (panel 4), and the S2GΔHR2-5GS-1TD0 spike purified on a CR3022 column (panel 5). SEC profiles for three separate production runs are shown for the $S2G_{ECTO}$-5GS-1TD0 spike. **(C)** Schematic representation of a SARS-CoV-2 spike on the virus surface in the presence of host ACE2 and the HR2 region from a neighboring spike (left) and sequence alignment of SARS-CoV-1/2 HR1 (right, top) and HR2 (right, bottom). The HR1 and HR2 regions that form the six-helix bundled in the post-fusion state are colored in green and brown, respectively. **(D)** Left: SEC profiles of S2GΔHR2-5GS-1TD0 from a Superose 6 10/300

GL column for four separate production runs. Right: BN-PAGE of $S2P_{ECTO}$-5GS-1TD0 and S2GΔHR2-5GS-1TD0. SEC fractions (12.5-14) are shown for S2GΔHR2-5GS-1TD0 on the gel. **(E)** ELISA binding of two SARS-CoV-2 spikes ($S2P_{ECTO}$-5GS-1TD0 and S2GΔHR2-5GS-1TD0) to five mAbs/NAbs. EC_{50} (μg/ml) values are labeled on the plot. **(F)** Octet binding of two SARS-CoV-2 spikes to five mAbs/NAbs. Sensorgrams were obtained from an Octet RED96 instrument at six antigen concentrations from 150 to 4.7nM by twofold dilution.

Fig. 3 Rational design of SARS-CoV-2 spike-presenting SApNP vaccines. (A) Schematic representation of SARS-CoV-2 virion (top) and spike-presenting SApNP vaccine (bottom). For the SARS-CoV-2 virion, pre/post-fusion S, nucleocapsid and RNA viral genome are labeled, while for the vaccine, stabilized spike and multilayered SApNP carrier are labeled. **(B)** Colored surface models of SApNP carriers (top) and spike-presenting SApNP vaccines (bottom). Three SApNP carriers shown here are 24-meric ferritin (FR) and 60-meric E2p and I3-01v9. SApNP size is indicated by diameter (in nanometers). **(C)** SEC profiles of SARS-CoV-2 S2GΔHR2 SApNPs obtained from a Superose 6 10/300 GL column for three separate production runs. **(D)** EM images of three SARS-CoV-2 spike SApNPs: S2GΔHR2-5GS-FR (left), S2GΔHR2-5GS-E2p-LD4-PADRE (or -L4P, middle), and S2GΔHR2-10GS-I3-01v9-LD7-PADRE (or -L7P, right). **(E)** ELISA binding of three SARS-CoV-2 spike SApNPs to five mAbs/NAbs. EC_{50} (μg/ml) values are labeled on the plot. **(F)** Antigenic profiles of SARS-CoV-2 S2GΔHR2 spike and three SApNPs against five mAbs/NAbs Sensorgrams were obtained from an Octet RED96 using six antigen concentrations (150-4.6nM for the spike, 9-0.27nM for the FR SApNP, and 3.5-0.1nM for the E2p and I3-01v9 SApNPs, respectively, all by twofold dilution) and quantitation biosensors, as shown in fig. S3B. The peak signals (nm) at the highest concentration are listed in the matrix. Color coding indicates the signal strength measured by Octet (green to red: low to high).

Fig. 4. SARS-CoV-1/2 vaccine-induced binding antibody response in mice. (A) Schematic representation of the mouse immunization protocol. **(B)** Longitudinal analysis of SARS-CoV-2 RBD/RBD-SApNP vaccine-induced binding antibody titers in mouse sera. The S2GΔHR2 spike vaccine group is included for comparison. ED_{50} titers (fold of dilution) calculated from ELISA binding of mouse sera to the coating antigens, SARS-CoV-2 S2GΔHR2-5GS-foldon (left) and RBD (Left). **(C)** Longitudinal analysis of SARS-CoV-2 spike/spike-SApNP vaccine-induced binding antibody titers in mouse sera. Top: ED_{50} titers calculated from ELISA binding of mouse sera to the coating antigen, SARS-CoV-2 S2GΔHR2-5GS-foldon. For the $S2P_{ECTO}$-5GS-1TD0 vaccine group, the $S2P_{ECTO}$-5GS-foldon spike was used as the coating antigen. Bottom: ED_{50} titers calculated from ELISA binding of mouse sera to the coating antigen, SARS-CoV-2 RBD. **(D)** Longitudinal analysis of SARS-CoV-1 vaccine-induced binding antibody titers in mouse sera. ED_{50} titers calculated from ELISA binding of mouse sera to the coating antigens, SARS-CoV-1 $S2P_{ECTO}$-5GS-foldon (left) and RBD (right). The *P*-values were determined by an unpaired *t* test in GraphPad Prism 8.4.3 with (*) indicating the level of statistical significance. Average ED_{50} values are labeled on the plots. Detailed serum ELISA data is shown in figs. S4-S6.

Fig. 5. SARS-CoV-1/2 vaccine-induced neutralizing antibody response in mice. (A) Longitudinal analysis of SARS-CoV-2 RBD/RBD-SApNP vaccine-induced neutralizing antibody titers in mouse sera. The S2GΔHR2 spike vaccine group is included for comparison. ID_{50} titers (fold of dilution) calculated from pseudovirus neutralization assays against SARS-CoV-2-pps (left) and SARS-CoV-1-pps (right). **(B)** Longitudinal analysis of SARS-CoV-2 spike/spike-SApNP vaccine-induced neutralizing antibody titers in mouse sera. ID_{50} titers calculated from pseudovirus neutralization assays against SARS-CoV-2-pps (top) and SARS-CoV-1-pps (bottom). **(C)** Longitudinal analysis of SARS-CoV-1 vaccine-induced neutralizing antibody titers in mouse

884 sera. ID_{50} titers calculated from pseudovirus neutralization assays against SARS-CoV-1-pps (left)
885 and SARS-CoV-2-pps (right). The *P*-values were determined by an unpaired *t* test in GraphPad
886 Prism 8.4.3 with (*) indicating the level of statistical significance. Average ED_{50} values are labeled
887 on the plots. Detailed serum SARS-CoV-1/2-pp neutralization data is shown in figs. S7-S9.

888 **Fig. 6. SARS-CoV-2 vaccine-induced T-cell responses in mice.** Splenocytes from mice (n=5 for
889 each group) immunized with the $S2P_{ECTO}$ spike, E2p SApNP or I3-01v9 SApNP were isolated at
890 w11, and cultured in the presence of IL-2 and DC-pulsed with the $S2P_{ECTO}$ spike (1×10^{-7} μM),
891 E2p SApNP (1×10^{-7} μM) or I3-01v9 SApNP (1×10^{-7} μM), correspondingly. Splenocytes from 5
892 naïve mice were used as the control samples and cultured in the presence of DCs without antigen-
893 pulsing. Cells were assessed after 16 hours (A, C) and 4 hours (B, D) of culture. **(A)** and **(B)**:
894 Vaccine-induced $CD4^+$ T cell immunity. **(C)** and **(D):** Vaccine-induced $CD8^+$ T cell immunity.
895 Plots show the frequencies of cell fraction. The *P* values were determined by one-way ANOVA
896 analysis. *, P<0.05; **, P<0.01; ***, P<0.001.

Figure 1

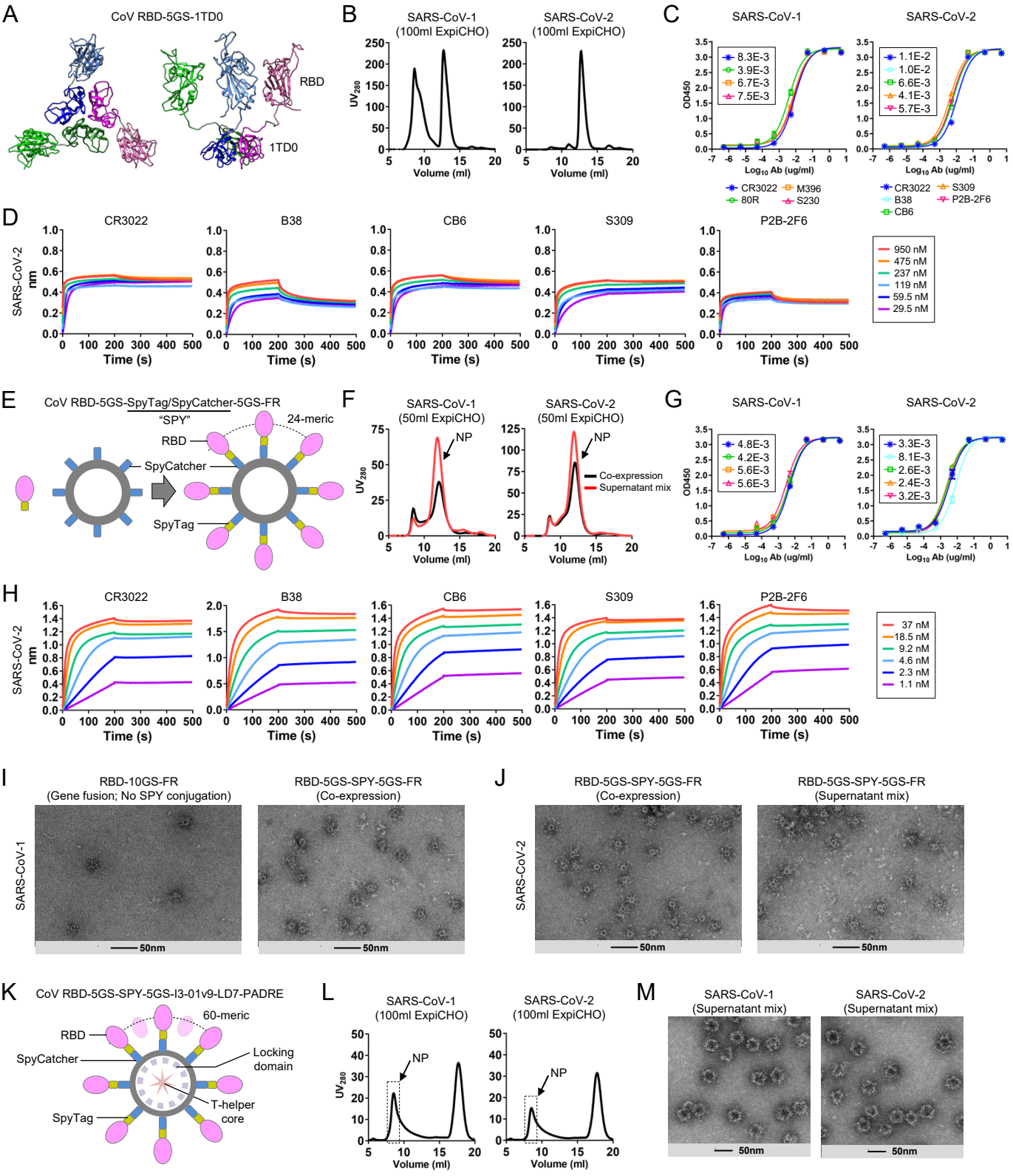

Figure 2

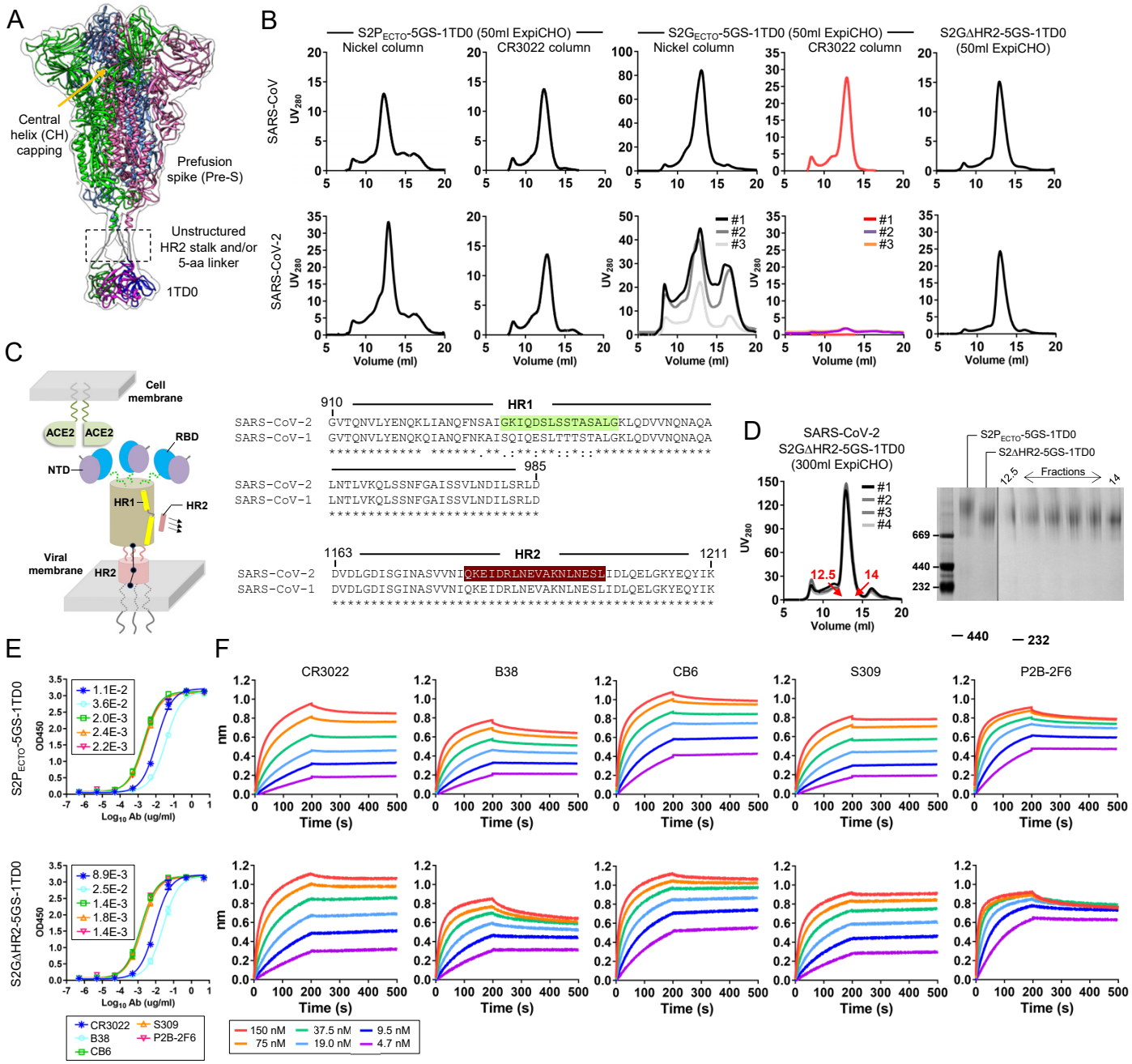

Figure 3

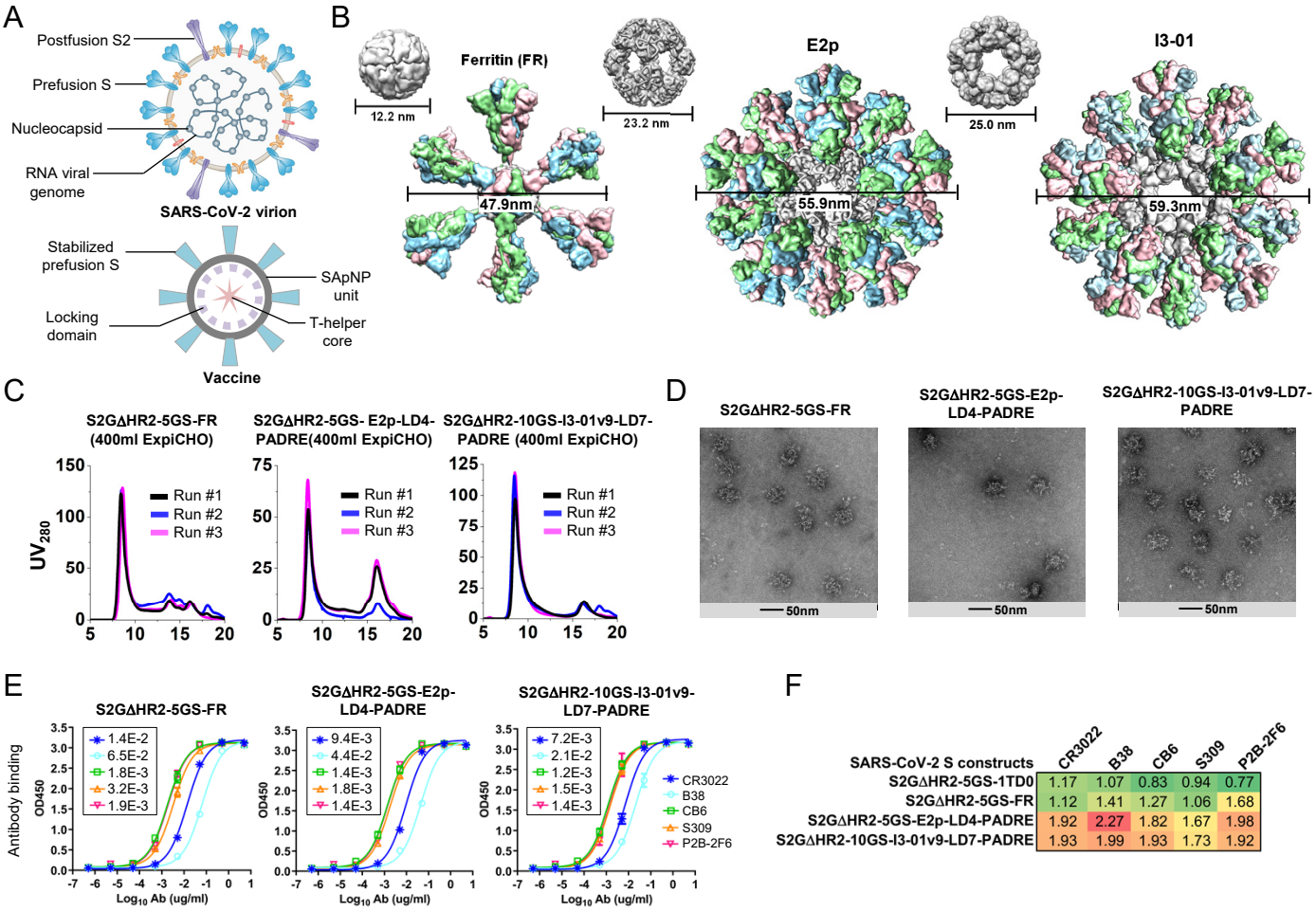

F

SARS-CoV-2 S constructs	CR3022	B38	CB6	S309	P2B-2F6
S2GΔHR2-5GS-1TD0	1.17	1.07	0.83	0.94	0.77
S2GΔHR2-5GS-FR	1.12	1.41	1.27	1.06	1.68
S2GΔHR2-5GS-E2p-LD4-PADRE	1.92	2.27	1.82	1.67	1.98
S2GΔHR2-10GS-I3-01v9-LD7-PADRE	1.93	1.99	1.93	1.73	1.92

Figure 4

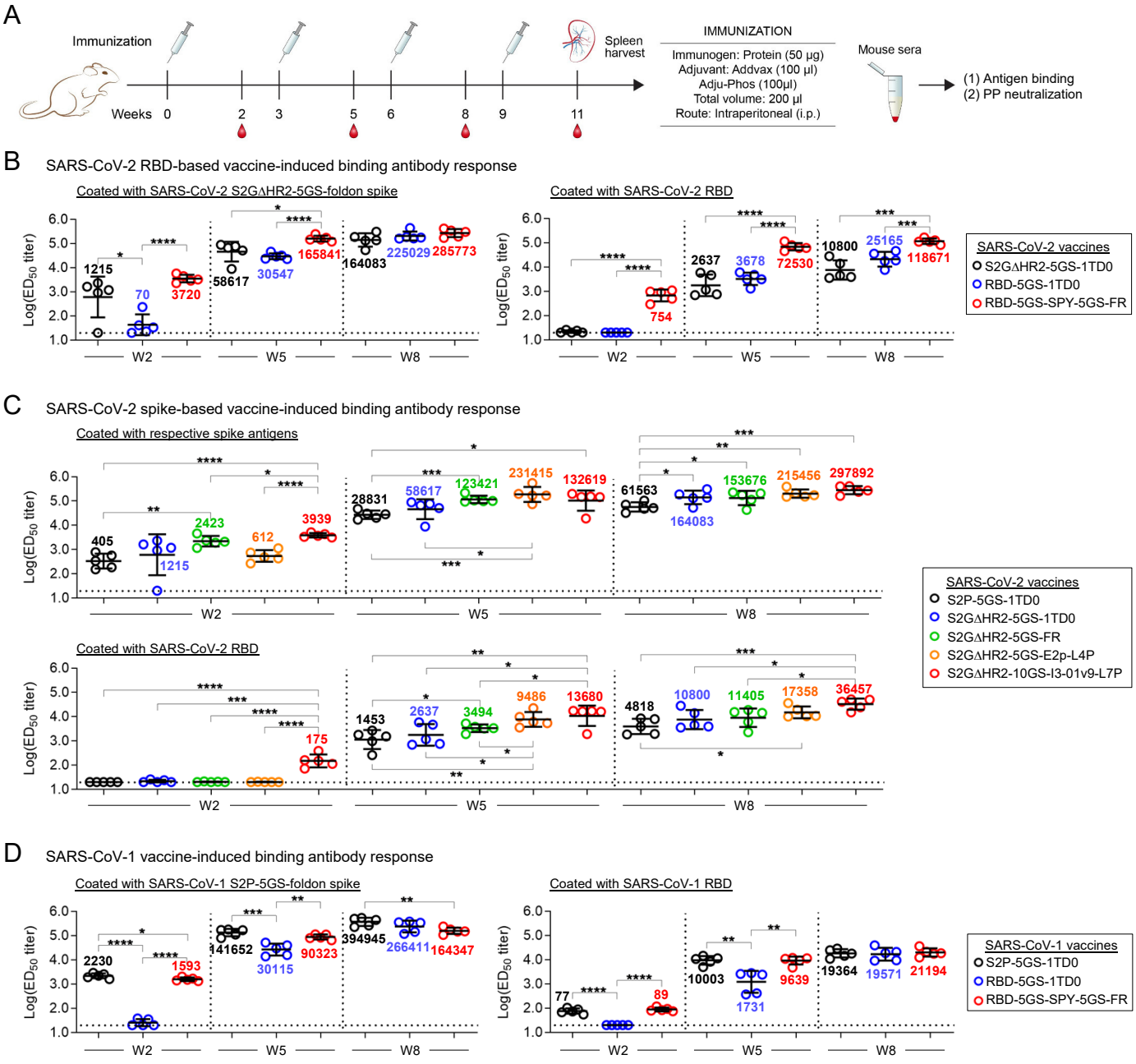

Figure 5

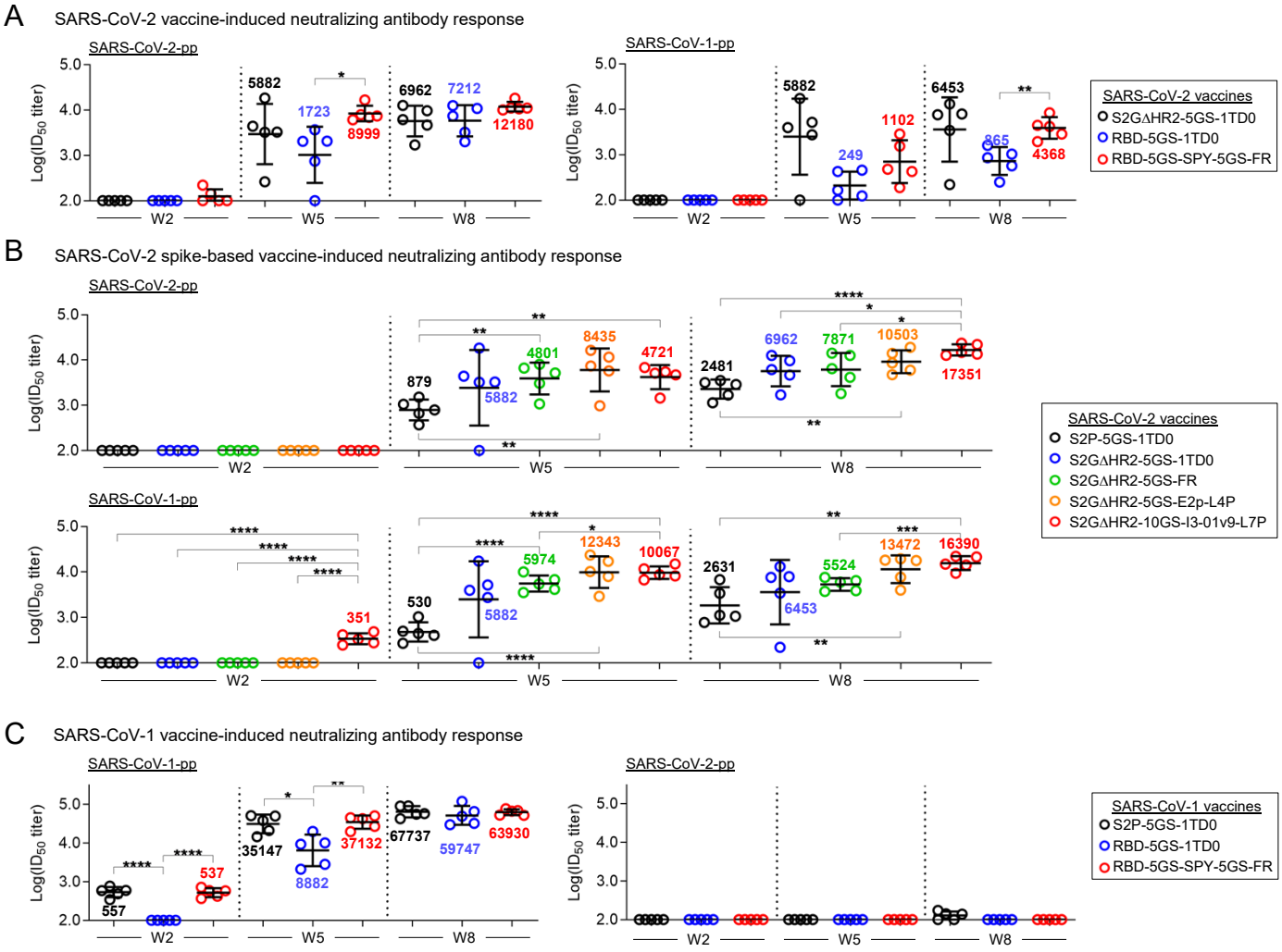

Figure 6

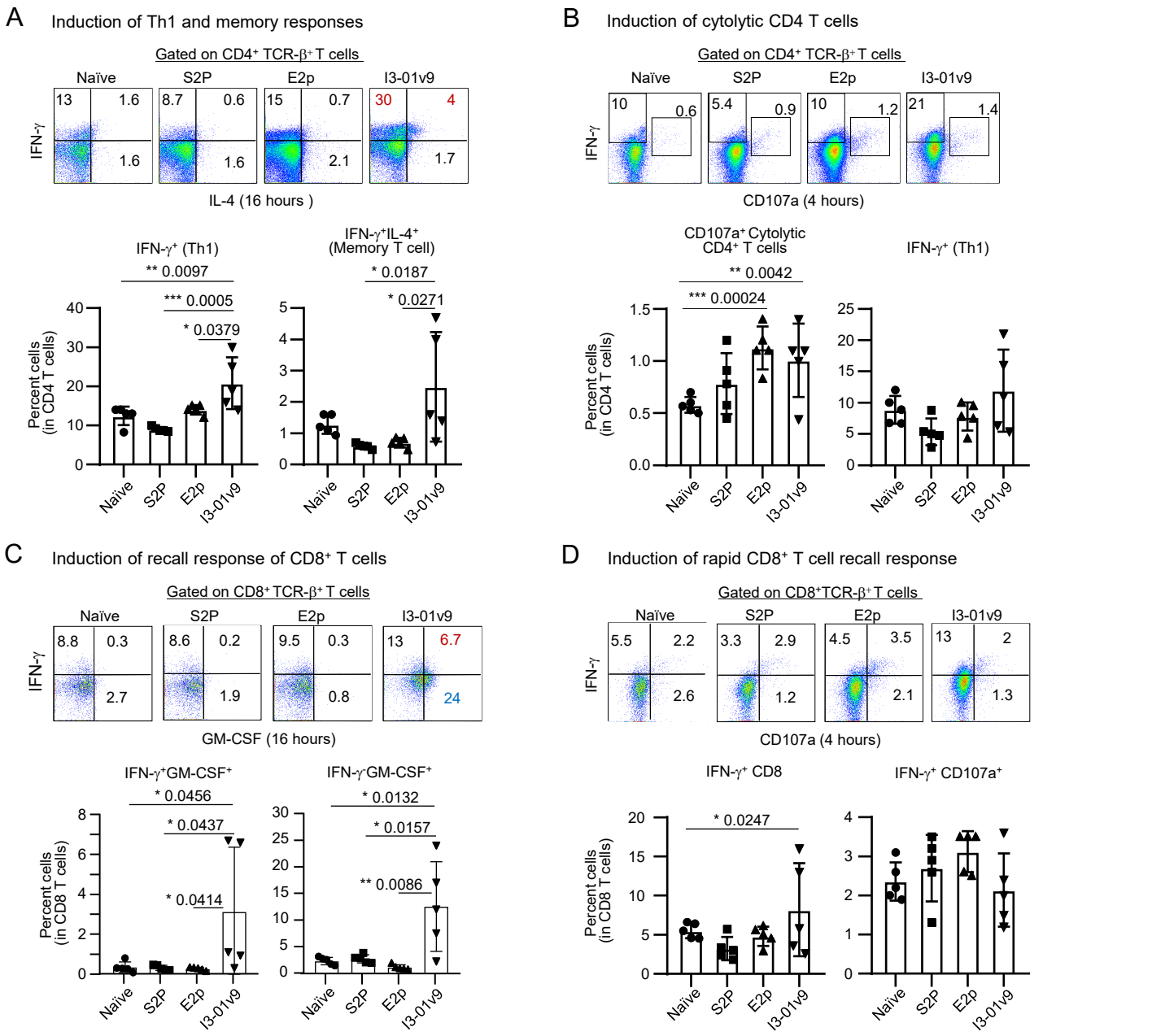

fig. S1

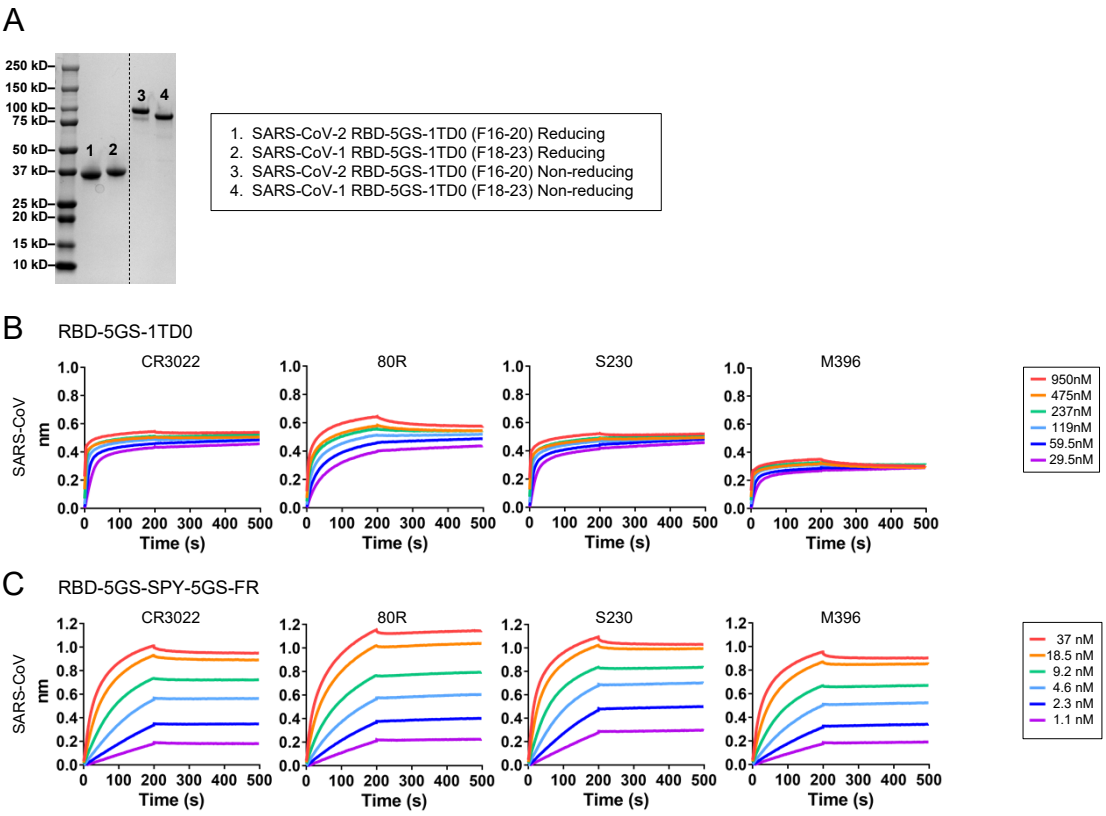

fig. S1. Characterization of SARS-CoV-1/2 RBD immunogens. (A) SDS-PAGE of purified SARS-CoV-1/2 RBD-5GS-1TD0 under the reducing and non-reducing conditions. The black dashed line indicates where a non-SARS-CoV-1/2 RBD protein analyzed on the same gel has been removed. **(B)** BLI profiles of SARS-CoV-1 RBD-5GS-1TD0 trimer binding to four antibodies. **(C)** BLI profiles of SARS-CoV-1 RBD-5GS-Spytag/SpyCatcher-5GS-FR SApNP binding to four antibodies. In **(B)** and **(C)**, sensorgrams were obtained from an Octet RED96 instrument using a series of six concentrations (950-29.5nM for the RBD trimer and 37-1.1nM for the RBD SApNP, respectively, both by twofold dilution) and kinetics biosensors.

fig. S2

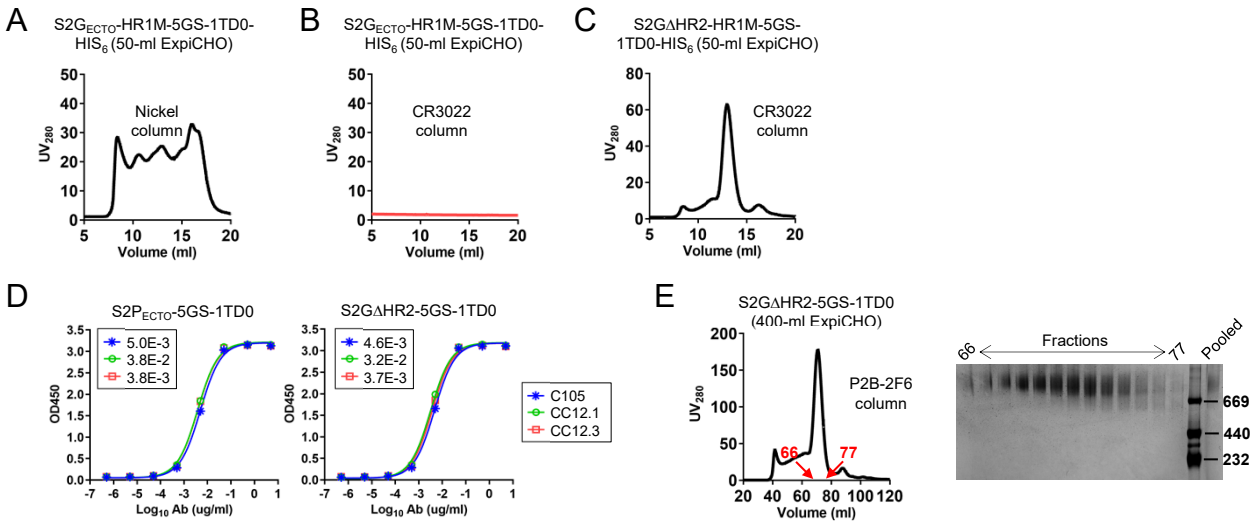

fig. S2. Characterization of SARS-CoV-2 spikes. (A) SEC profile of an S2G$_{ECTO}$-5GS-1TD0 construct in which the HR1 region (L922-S943) is replaced by the equivalent SARS-CoV-1 HR1 region (termed S2G$_{ECTO}$-HR1M-5GS-1TD0-HIS$_6$). The construct was transiently expressed in 50ml ExpiCHO cells and purified on a Nickel column before SEC. **(B)** SEC profile of S2G$_{ECTO}$-HR1M-5GS-1TD0-HIS$_6$ following transient expression in 50ml ExpiCHO cells and purification on a CR3022 column. **(C)** SEC profile of S2GΔHR2-HR1M-5GS-1TD0-HIS$_6$ following transient expression in 50ml ExpiCHO cells and purification on a CR3022 column. **(D)** ELISA curves of SARS-CoV-2 S2P$_{ECTO}$-5GS-1TD0 and S2GΔHR2-5GS-1TD0 binding to three newly identified potent human NAbs, C105, CC12.1, and CC12.3. **(E)** Left: SEC profile of S2GΔHR2-5GS-1TD0 obtained from a HiLoad 16/600 Superose 6 column following transient expression in 400-ml ExpiCHO cells and purification on a P2B-2F6 antibody column. The range of fractions used for the BN-PAGE analysis is indicated on the SEC profile.; Right: BN-PAGE of SEC fractions (66-77ml) and pooled fractions.

fig. S3

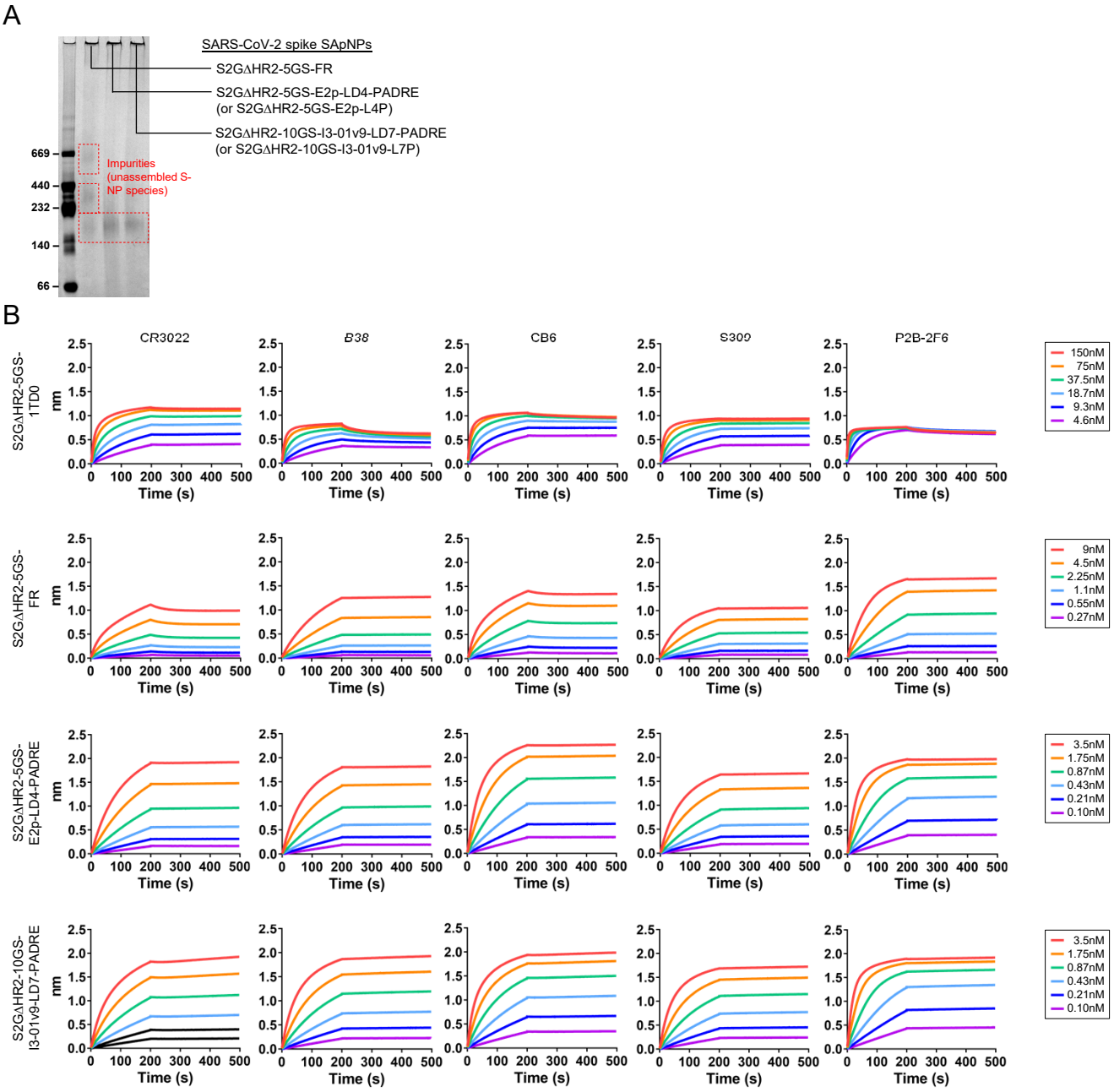

fig. S3. Characterization of SARS-CoV-2 S2GΔHR2 SApNPs. (A) BN-PAGE of CR3022-purified S2GΔHR2-presenting SApNPs. Due to the large size and molecular mass, SApNPs would be in the well on the top of the gel, whereas the unassembled species would be seen on the gel. **(B)** BLI profiles of SARS-CoV-2 S2GΔHR2-presenting SApNPs binding to five antibodies**.** The SARS-CoV-2 S2GΔHR2-5GS-1TD0 trimer was included for comparison. Sensorgrams were obtained from an Octet RED96 instrument using a series of six concentrations (150-4.6nM for the S2GΔHR2 trimer, 9-0.27nM for the FR SApNP, and 3.5-0.1nM for the E2p and I3-01v9 SApNPs, respectively, all by twofold dilution) and quantitation biosensors.

fig. S4

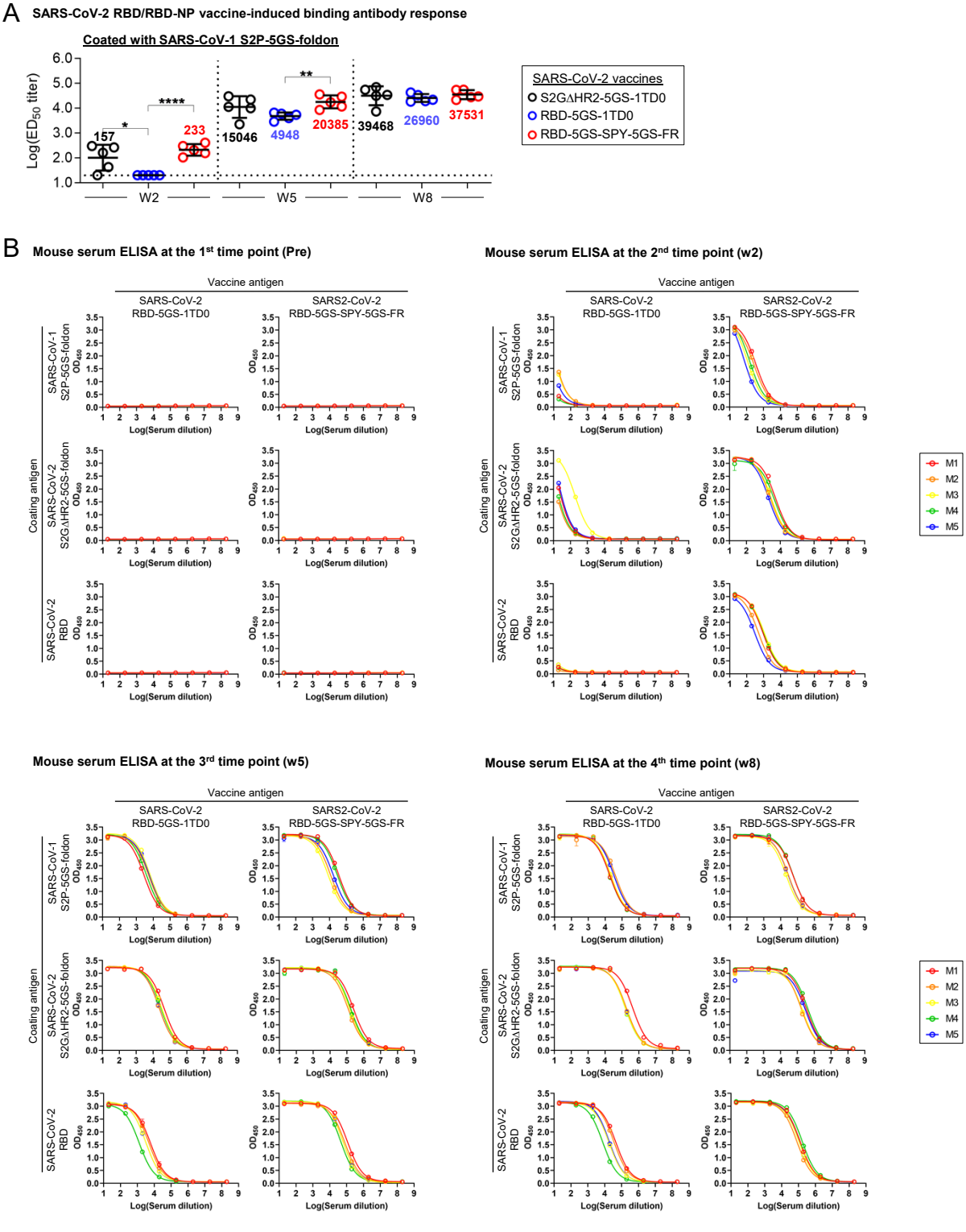

fig. S4

Mouse serum ELISA at the 5th time point (w11)

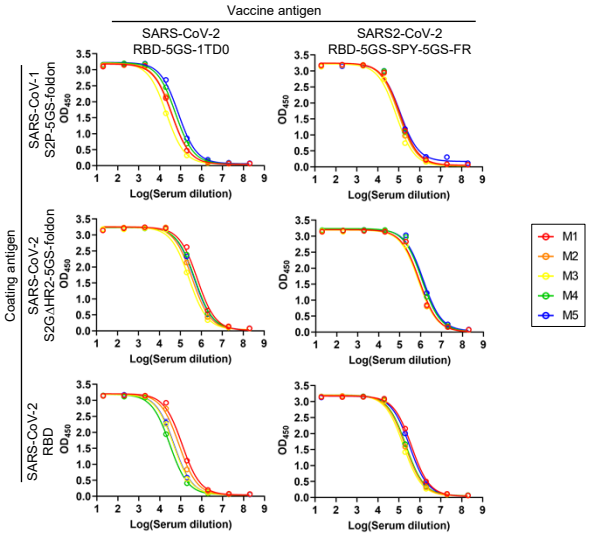

C **Mouse serum ELISA ED_{50} values**

Coating antigen	SARS-CoV-2 vaccine antigen	w2					w5					w8					w11				
		M1	M2	M3	M4	M5	M1	M2	M3	M4	M5	M1	M2	M3	M4	M5	M1	M2	M3	M4	M5
SARS-CoV-1 S2P-5GS-foldon	SARS-CoV-2 RBD-5GS-1TD0	<20	<20	<20	<20	<20	2849	5426	6544	4016	5908	18964	42380	21799	18353	33308	37799	38906	21152	57386	77425
	SARS-CoV-2 RBD-5GS-SPY-5GS-FR	402	299	155	205	105	35702	11730	8478	28869	17148	55019	29258	21429	54316	27631	116637	100384	75563	114456	117834
SARS-CoV-2 S2GΔHR2-5GS-foldon	SARS-CoV-2 RBD-5GS-1TD0	33	<20	237	23	41	45821	22822	31754	28895	23447	437779	186022	163880	159780	177684	640237	365517	258393	495393	458394
	SARS-CoV-2 RBD-5GS-SPY-5GS-FR	5719	2893	3239	4472	2280	245016	119447	145979	172388	146375	343504	169804	194569	415264	305726	893358	866269	801461	1181201	1352045
SARS-CoV-2 RBD	SARS-CoV-2 RBD-5GS-1TD0	<20	<20	<20	<20	<20	6061	4770	3127	1293	3140	46119	35578	17646	7671	18814	116486	82504	45221	30347	47738
	SARS-CoV-2 RBD-5GS-SPY-5GS-FR	913	499	1092	978	292	115261	78765	61890	45215	61522	125683	81629	110472	165129	110446	402781	200112	165137	217751	328643

fig. S4. SARS-CoV-2 RBD/RBD-NP vaccine-induced binding antibody response. (A) Plot of ED_{50} titers (fold of dilution) calculated from ELISA binding of mouse sera from two SARS-CoV-2 RBD-based vaccine groups (RBD-5GS-1TD0 and RBD-5GS-SPY-5GS-FR) to the coating antigen, SARS-CoV-1 S2P-5GS-foldon, with the SARS-CoV-2 spike vaccine group (S2GΔHR2-5GS-1TD0) included for comparison. *P*-values were determined by an unpaired *t* test in GraphPad Prism 8.4.3 with (*) indicating the level of statistical significance (*: $0.01<P\leq0.05$; **: $0.001<P\leq0.01$; ***: $0.0001<P\leq0.001$; ****: $P\leq0.0001$). **(B)** ELISA binding curves of mouse sera from two SARS-CoV-2 RBD-based vaccine groups to three coating antigens, SARS-CoV-1 S2P-5GS-foldon, SARS-CoV-2 S2GΔHR2-5GS-foldon, and SARS-CoV-2 RBD. **(C)** Summary of ED_{50} titers measured for two SARS-CoV-2 RBD-based vaccine groups against three coating antigens. Color coding indicates the level of ED_{50} titer (white: no binding; green to red: low to high). The ED_{50} values were calculated in GraphPad Prism 8.4.3. Of note, the ED_{50} values at w2 were derived by setting the lower/upper constraints of OD_{450} at 0.0/3.2 to achieve greater accuracy.

fig. S5

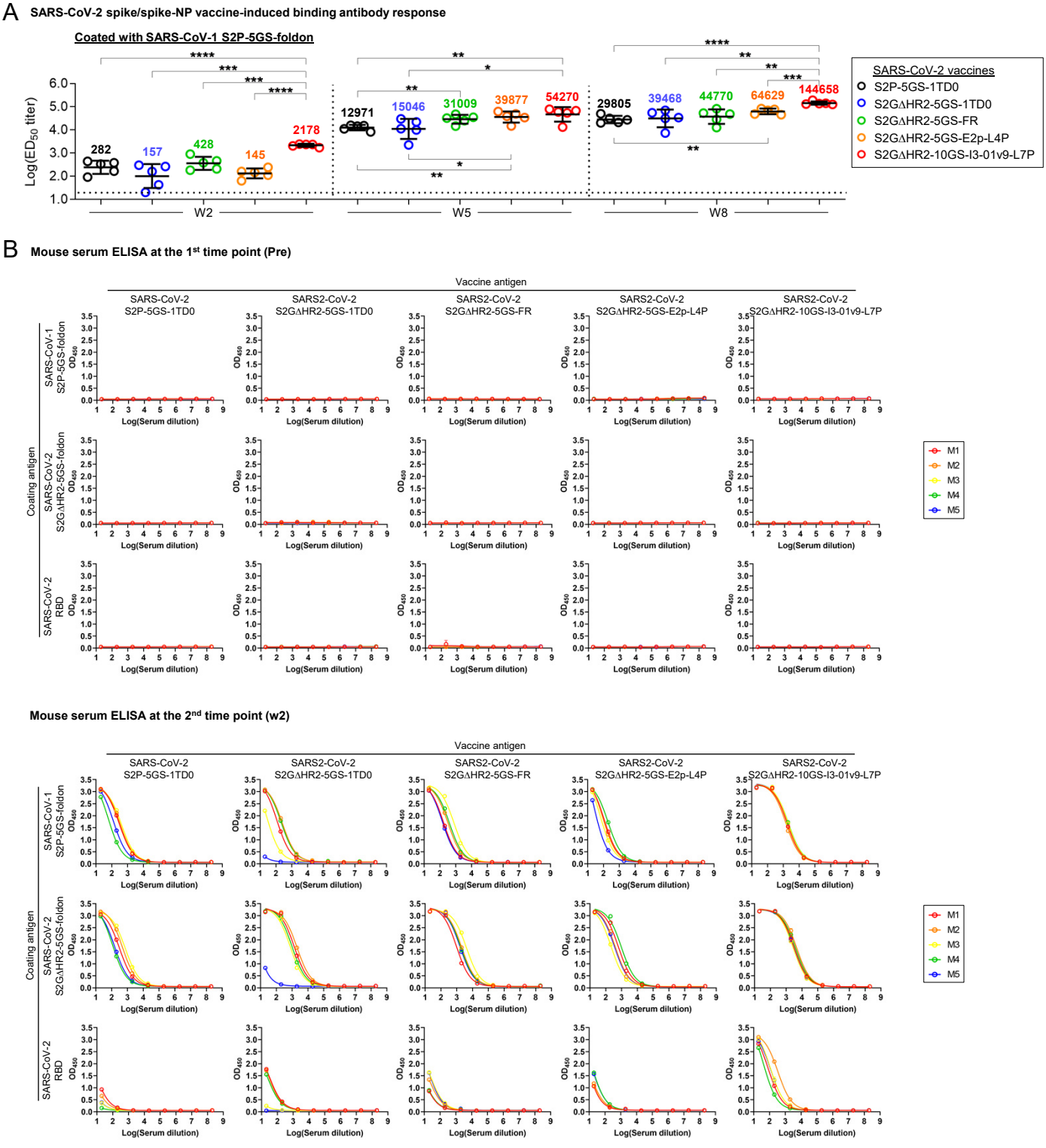

fig. S5

Mouse serum ELISA at the 3rd time point (w5)

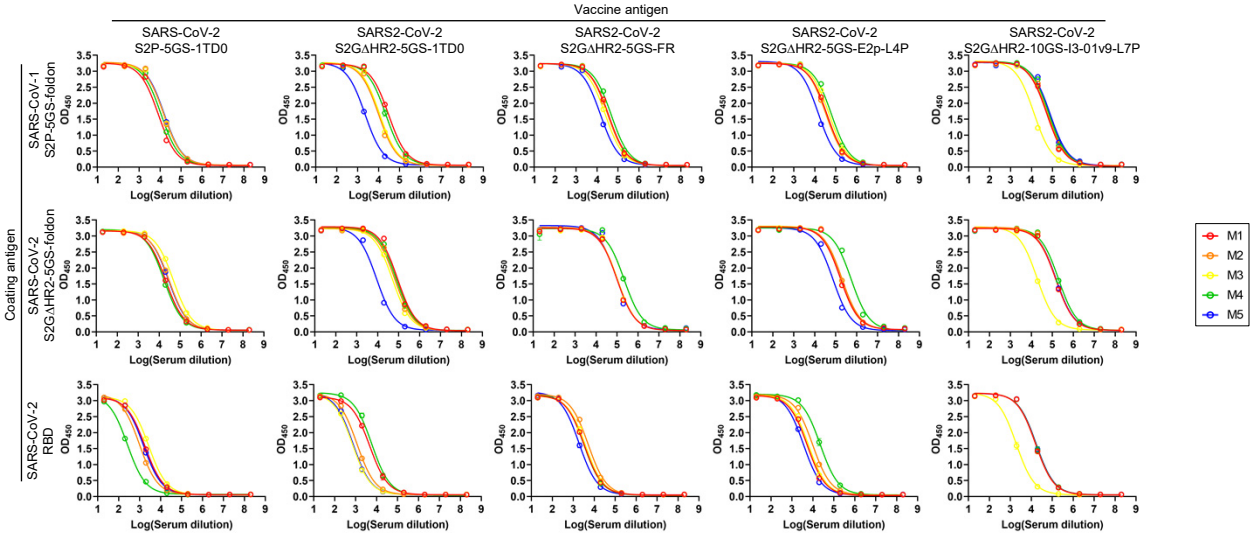

Mouse serum ELISA at the 4th time point (w8)

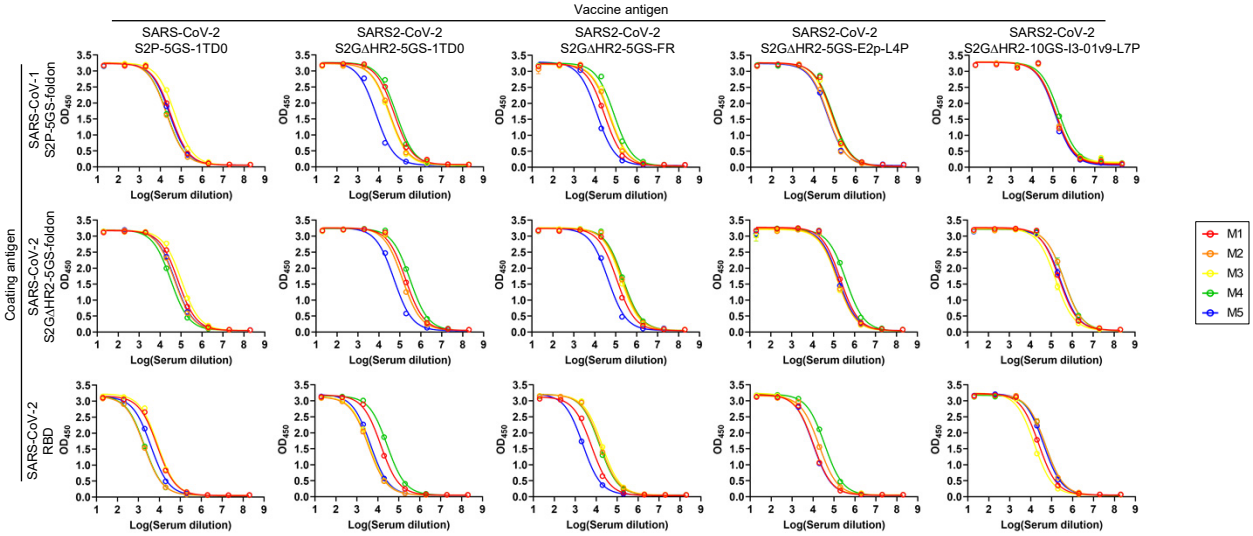

fig. S5

Mouse serum ELISA at the 5th time point (w11)

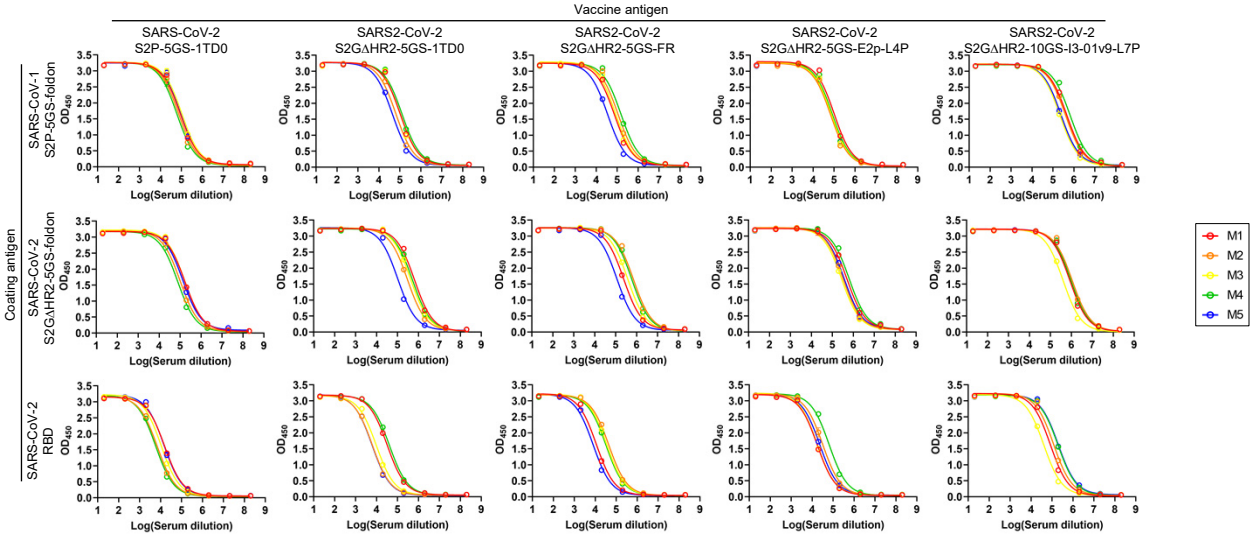

C **Mouse serum ELISA ED_{50} values**

Coating antigen	SARS-CoV-2 vaccine antigen	w2					w5					w8					w11				
		M1	M2	M3	M4	M5	M1	M2	M3	M4	M5	M1	M2	M3	M4	M5	M1	M2	M3	M4	M5
SARS-CoV-1 S2P-5GS-foldon	S2P-5GS-1TD0	337	378	438	92	166	8229	14598	15271	11029	15730	31346	19923	49495	20899	27362	87963	74675	105473	61814	98729
	S2GDHR2-5GS-1TD0	160	300	43	264	<20	29889	9934	11211	21972	2225	54736	33977	31597	69701	7331	104856	65140	102307	125912	44213
	S2GDHR2-5GS-FR	207	379	907	463	182	35236	32621	25025	47534	14631	28314	48030	53004	81962	12542	73512	110204	85157	152546	35108
	S2GDHR2-5GS-E2p-L4P	161	145	111	244	64	38631	34068	49277	62620	14788	76610	48384	69459	83674	45019	101670	68765	75147	83008	78758
	S2GDHR2-10GS-I3-01v9-L7P	2047	1697	2368	2434	2342	53863	59267	13164	67367	77688	136410	139928	130590	190016	126344	461522	400892	212809	662353	240540
SARS-CoV-2 S2GΔHR2-5GS-foldon	S2P-5GS-1TD0	342	564	786	152	186	20525	30418	47919	16989	28307	71336	48544	104033	32473	51430	168104	101372	164947	77599	136078
	S2GDHR2-5GS-1TD0	1623	2329	915	1190	<20	88704	66897	51587	77015	8882	188541	133257	137492	308124	53005	648885	297906	427211	524920	103434
	S2GDHR2-5GS-FR	1168	2365	4609	2102	1925	100424	99021	105640	217243	94779	112191	207821	177619	227282	43471	240083	710983	381026	592260	116127
	S2GDHR2-5GS-E2p-L4P	748	481	268	1132	435	168389	197689	167303	549503	74194	209083	153974	150854	389845	173525	500160	324937	276279	631496	369062
	S2GDHR2-10GS-I3-01v9-L7P	3695	5177	3135	4338	3353	147140	146498	19018	197789	152653	239618	402217	162393	412328	272905	843216	1100695	403762	949208	944347
SARS-CoV-2 RBD	S2P-5GS-1TD0	<20	<20	<20	<20	<20	1801	980	2693	260	1533	7881	1861	8448	1952	3948	15828	6935	10668	5826	14807
	S2GDHR2-5GS-1TD0	26	24	<20	<20	<20	4693	1161	703	5881	751	13835	3578	3906	28190	4493	32268	6328	9751	40928	6118
	S2GDHR2-5GS-FR	<20	<20	22	<20	21	3340	5205	3799	3229	1900	5996	15596	18918	14222	2293	11360	44589	35885	32606	7947
	S2GDHR2-5GS-E2p-L4P	<20	<20	<20	21	<20	5425	9801	6186	22466	3554	10682	19414	10367	36238	10091	17641	32324	17662	64941	23122
	S2GDHR2-10GS-I3-01v9-L7P	112	384	159	73	151	16265	16054	1920	16797	17368	24415	49820	15026	51700	41325	84065	120318	40866	194224	199672

fig. S5. SARS-CoV-2 spike/spike-NP vaccine-induced binding antibody response. (A) Plot of ED_{50} titers (fold of dilution) calculated from ELISA binding of mouse sera from five SARS-CoV-2 spike-based vaccine groups (S2P-5GS-1TD0, S2GΔHR2-5GS-1TD0, S2GΔHR2-5GS-FR, S2GΔHR2-5GS-E2p-L4P, and S2GΔHR2-10GS-I3-01v9-L7P) to the coating antigen, SARS-CoV-1 S2P-5GS-foldon. *P*-values were determined by an unpaired *t* test in GraphPad Prism 8.4.3 with (*) indicating the level of statistical significance (*: 0.01<P≤0.05; **: 0.001<P≤0.01; ***: 0.0001<P≤0.001; ****: P≤0.0001). **(B)** ELISA binding curves of mouse sera from five SARS-CoV-2 spike-based vaccine groups to three coating antigens, SARS-CoV-1 S2P-5GS-foldon, SARS-CoV-2 S2GΔHR2-5GS-foldon, and SARS-CoV-2 RBD. **(C)** Summary of ED_{50} titers measured for five SARS-CoV-2 spike-based vaccine groups against three coating antigens. Color coding indicates the level of ED_{50} titer (white: no binding; green to red: low to high). The ED_{50} values were calculated in GraphPad Prism 8.4.3. Of note, the ED_{50} values at w2 were derived by setting the lower/upper constraints of OD_{450} at 0.0/3.2 to achieve greater accuracy.

fig. S6

A

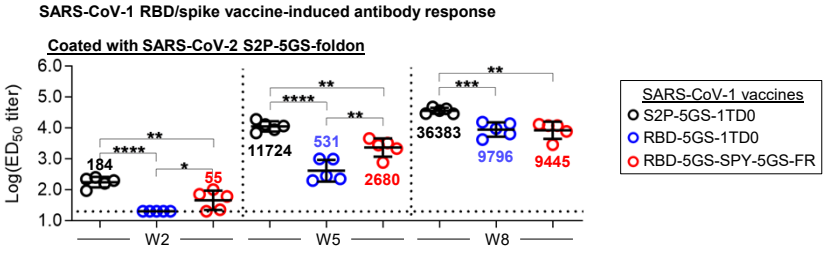

B

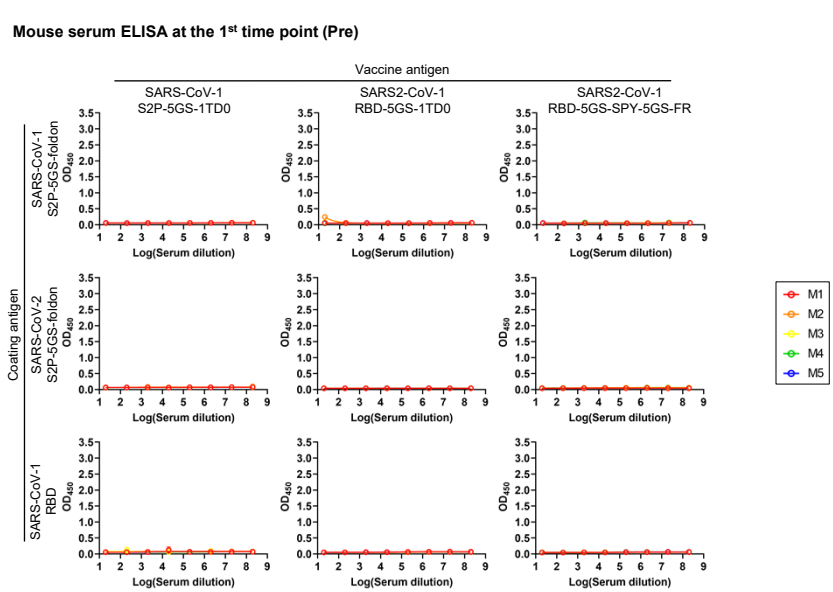

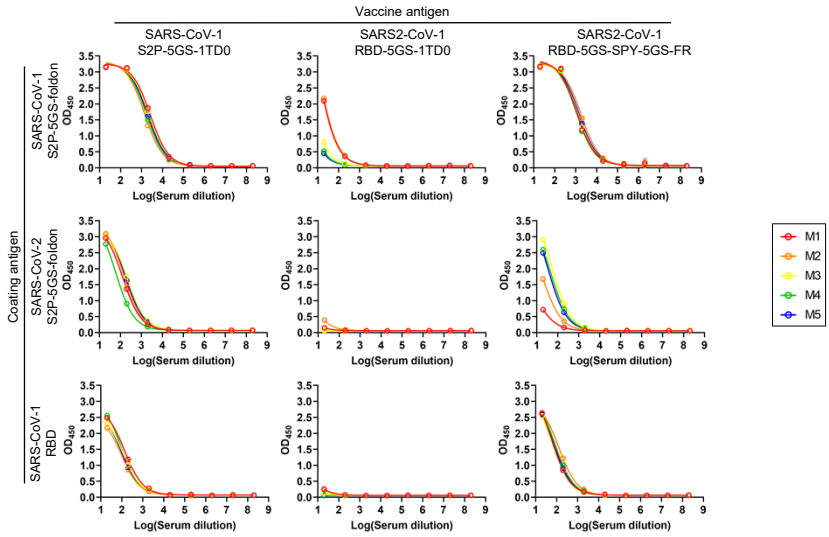

fig. S6

Mouse serum ELISA at the 3rd time point (w5)

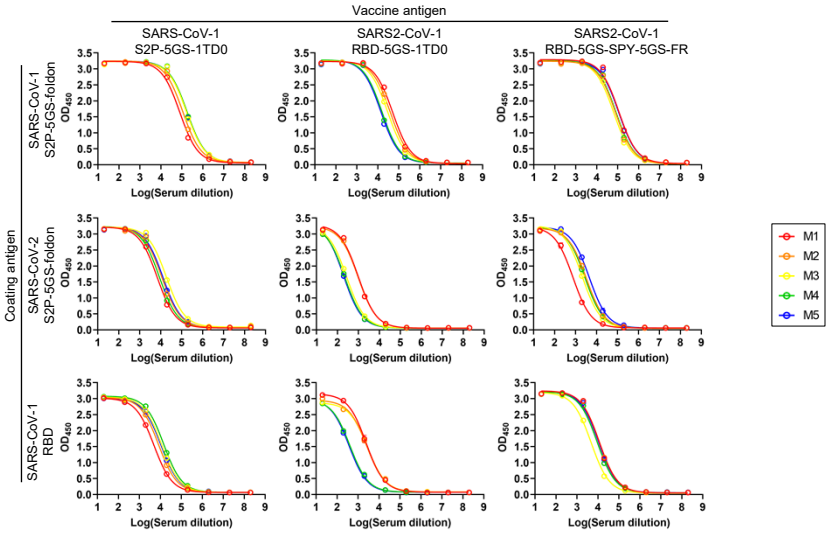

Mouse serum ELISA at the 4th time point (w8)

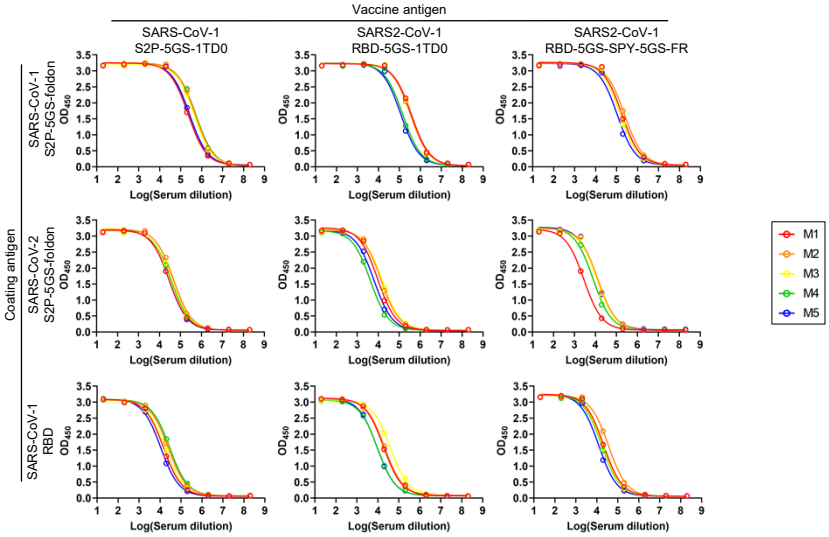

fig. S6

Mouse serum ELISA at the 5th time point (w11)

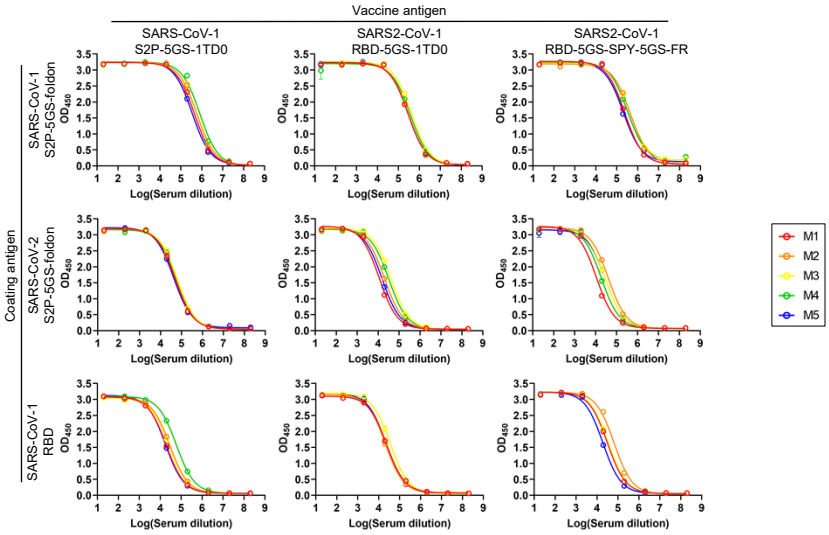

C

Mouse serum ELISA ED_{50} values

Coating antigen	SARS-CoV-1 vaccine antigen	w2					w5					w8					w11				
		M1	M2	M3	M4	M5	M1	M2	M3	M4	M5	M1	M2	M3	M4	M5	M1	M2	M3	M4	M5
SARS-CoV-1 S2P-5GS-foldon	S2P-5GS-1TD0	2874	1611	2546	1924	2196	79871	111383	167209	179036	170765	226510	499160	444229	539886	264941	449939	577309	607415	818477	352607
	RBD-5GS-1TD0	35	38	<20	<20	<20	51448	39666	29849	15658	13955	378373	337915	353896	144261	117614	290621	294825	425889	370917	290601
	RBD-5GS-SPY-5GS-FR	1410	2047	1496	1320	1692	113510	78891	64381	83234	111601	178346	237355	151022	147743	107270	242440	454498	412469	328237	204991
SARS-CoV-2 S2P-5GS-foldon	S2P-5GS-1TD0	159	196	251	92	222	6913	11383	18692	8754	12877	28975	47458	41115	36059	28310	49277	52192	62700	60806	42133
	RBD-5GS-1TD0	<20	<20	<20	<20	<20	985	975	274	224	197	9476	13677	15302	4216	6307	11223	20517	40915	32465	15295
	RBD-5GS-SPY-5GS-FR	<20	22	100	70	60	751	3243	2124	2768	4513	2840	13086	11753	7693	11851	10886	40615	28253	18689	29739
SARS-CoV-1 RBD	S2P-5GS-1TD0	104	55	73	89	68	4967	8355	11547	14466	10683	14673	24576	17828	28878	10869	19455	28689	26660	58793	17679
	RBD-5GS-1TD0	<20	<20	<20	<20	<20	2446	2600	2827	415	371	18820	20963	39469	9503	9100	24044	20641	35559	36058	22822
	RBD-5GS-SPY-5GS-FR	79	118	74	94	83	11483	11758	4772	9294	10888	21284	36104	18587	17645	12351	31380	66025	34973	34373	19241

fig. S6. SARS-CoV-1 spike/RBD/RBD-NP vaccine-induced binding antibody response. (A) Plot of ED_{50} titers (fold of dilution) calculated from ELISA binding of mouse sera from three SARS-CoV-1 vaccine groups (S2P-5GS-1TD0, RBD-5GS-1TD0, and RBD-5GS-SPY-5GS-FR) to the coating antigen, SARS-CoV-2 S2P-5GS-foldon. *P*-values were determined by an unpaired *t* test in GraphPad Prism 8.4.3 with (*) indicating the level of statistical significance (*: 0.01<P≤0.05; **: 0.001<P≤0.01; ***: 0.0001<P≤0.001; ****: P≤0.0001). **(B)** ELISA binding curves of mouse sera from three SARS-CoV-1 vaccine groups to three coating antigens, SARS-CoV-1 S2P-5GS-foldon, SARS-CoV-2 S2P-5GS-foldon, and SARS-CoV-1 RBD. **(C)** Summary of ED_{50} titers measured for three SARS-CoV-1 vaccine groups against three coating antigens. Color coding indicates the level of ED_{50} titer (white: no binding; green to red: low to high). The ED_{50} values were calculated in GraphPad Prism 8.4.3. Of note, the ED_{50} values at w2 were derived by setting the lower/upper constraints of OD_{450} at 0.0/3.2 to achieve greater accuracy.

fig. S7

A

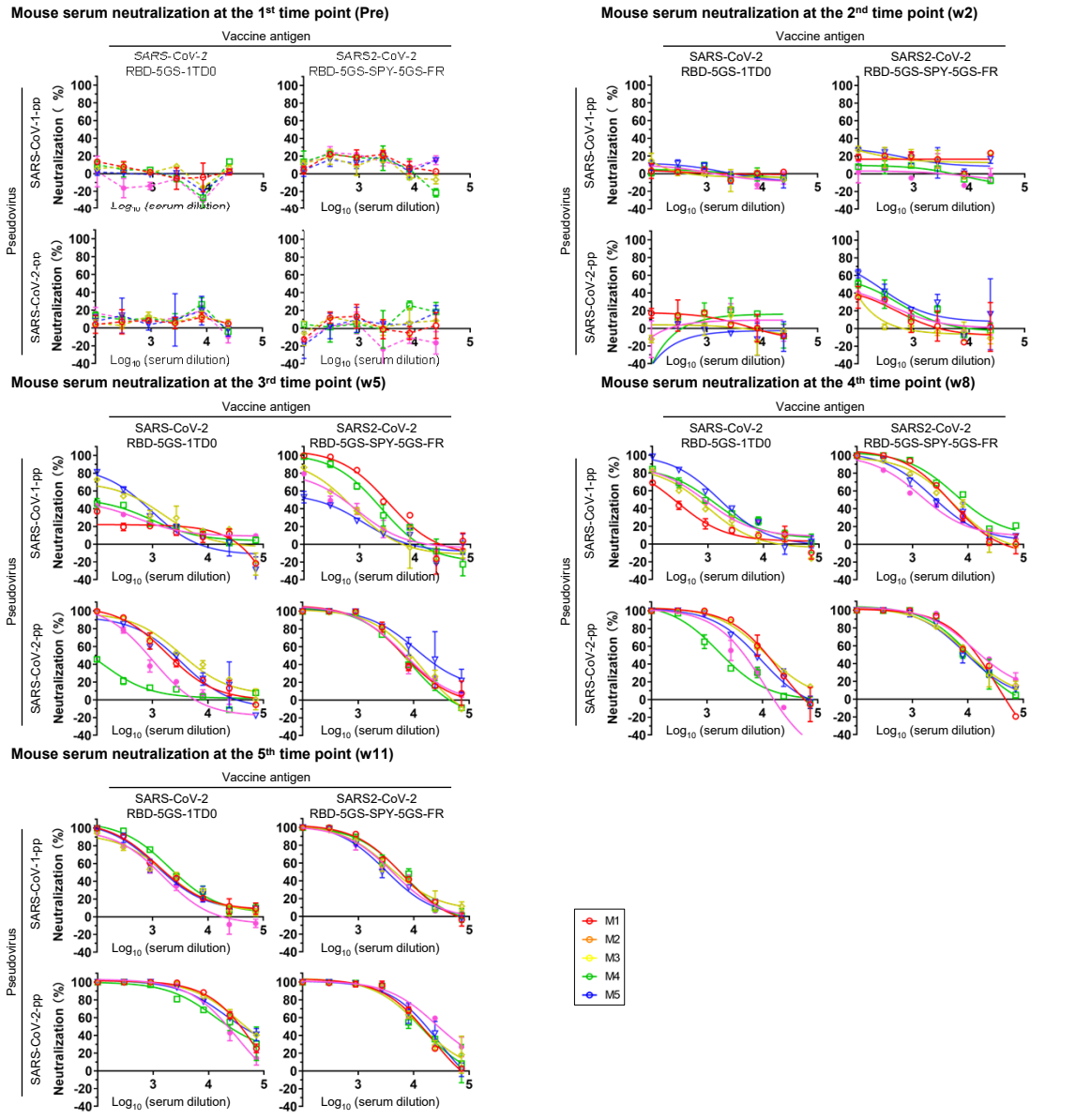

B

Mouse serum neutralization ID_{50} values

Pseudovirus: SARS-CoV-1-pp

SARS-CoV-2 vaccine antigen	W2					W5					W8					W11				
	M1	M2	M3	M4	M5	M1	M2	M3	M4	M5	M1	M2	M3	M4	M5	M1	M2	M3	M4	M5
RBD-5GS-1TD0	<100	<100	<100	<100	<100	72	428	459	166	124	250	570	1608	1037	859	1979	1710	1816	2759	1183
RBD-5GS-SPY-5GS-FR	<100	<100	<100	<100	<100	2870	482	189	1543	427	4456	4199	2858	8390	1941					

Pseudovirus: SARS-CoV-2-pp

SARS-CoV-2 vaccine antigen	W2					W5					W8					W11				
	M1	M2	M3	M4	M5	M1	M2	M3	M4	M5	M1	M2	M3	M4	M5	M1	M2	M3	M4	M5
RBD-5GS-1TD0	<100	<100	<100	<100	<100	2069	3655	2043	<100	746	10882	12545	7382	2010	3245	37249	46942	39750	25063	21536
RBD-5GS-SPY-5GS-FR	<100	<100	220	143	<100	6923	7926	16669	6079	7400	11048	11051	10012	10613	18178					

fig. S7. SARS-CoV-2 RBD/RBD-NP vaccine-induced neutralizing antibody response. (A) Pseudovirus neutralization curves of mouse sera from two SARS-CoV-2 RBD-based vaccine groups against two pseudoviruses, SARS-CoV-1-pp and SARS-CoV-2-pp. **(B)** Summary of ID_{50} titers measured for two SARS-CoV-2 RBD-based vaccine groups against two pseudoviruses. Color coding indicates the level of ID_{50} titer (white: no binding; green to red: low to high). The ID_{50} values were calculated in GraphPad Prism 8.4.3, with the lower/upper constraints of %neutralization set at 0.0/100.0.

fig. S8

A

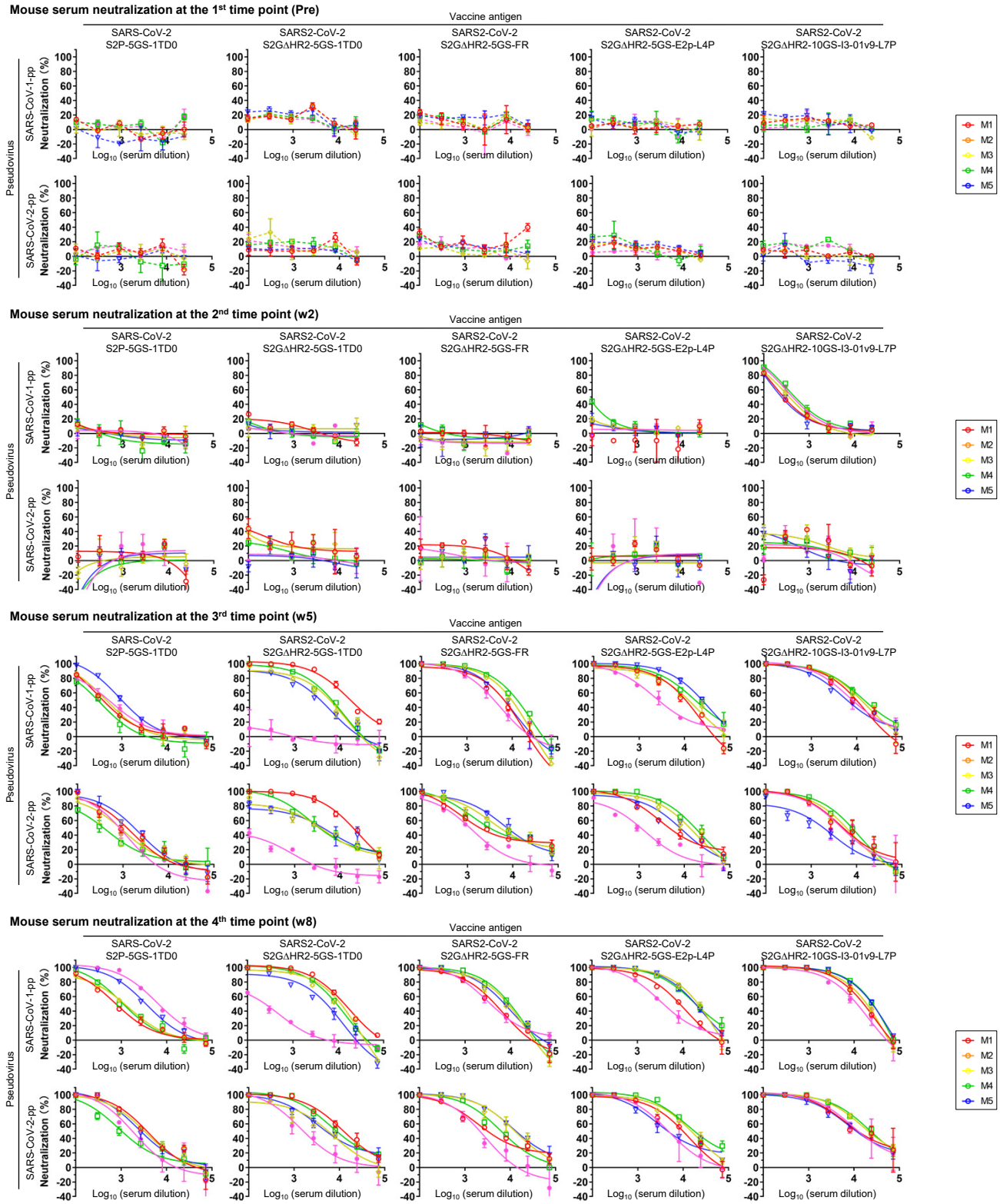

fig. S8

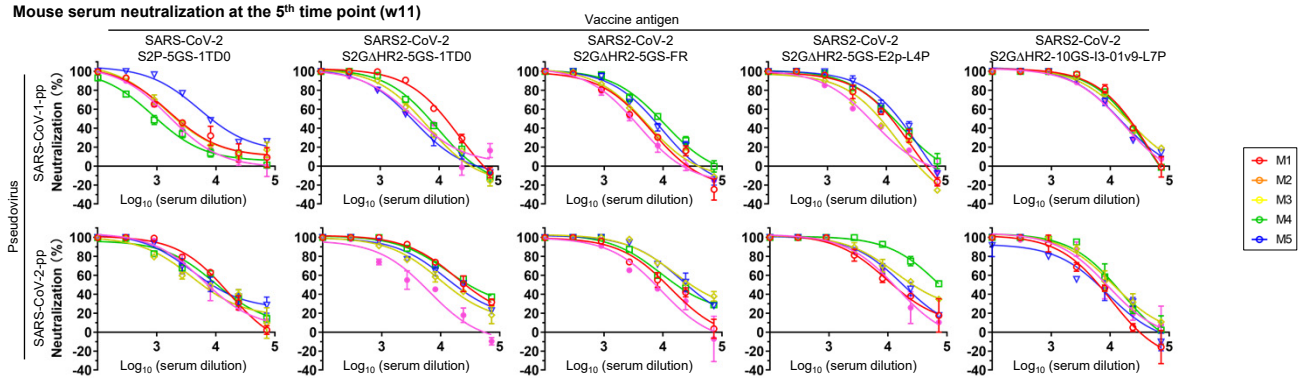

B

Mouse serum neutralization ID_{50} values

Pseudovirus: SARS-CoV-1-pp

SARS-CoV-2 vaccine antigen	W2					W5					W8					W11				
	M1	M2	M3	M4	M5	M1	M2	M3	M4	M5	M1	M2	M3	M4	M5	M1	M2	M3	M4	M5
S2P-5GS-1TD0	<100	<100	<100	<100	<100	405	444	1032	270	501	777	1062	3410	1121	6783	2588	2431	9374	1074	1806
S2GDHR2-5GS-1TD0	<100	<100	<100	<100	<100	17433	3960	2747	5170	<100	13124	7579	3443	7902	221	11228	4377	3271	6009	4176
S2GDHR2-5GS-FR	<100	<100	<100	<100	<100	4152	6773	5414	10007	3527	3735	5968	6443	7605	3872	3384	4103	5704	8194	2697
S2GDHR2-5GS-E2p-L4P	<100	<100	<100	<100	<100	7954	10197	23509	17140	2915	7676	18213	17917	19538	4017	9170	5651	13334	12484	4799
S2GDHR2-10GS-I3-01v9-L7P	278	330	247	486	417	8250	11666	6695	15034	8694	14174	14888	22024	21474	9393	18257	18901	14175	17014	13137

Pseudovirus: SARS-CoV-2-pp

SARS-CoV-2 vaccine antigen	w2					w5					w8					w11				
	M1	M2	M3	M4	M5	M1	M2	M3	M4	M5	M1	M2	M3	M4	M5	M1	M2	M3	M4	M5
S2P-5GS-1TD0	<100	<100	<100	<100	<100	1050	787	1524	369	667	3515	3169	2897	1141	1683	11358	7358	10878	10723	7868
S2GDHR2-5GS-1TD0	<100	<100	<100	<100	<100	18419	3271	3238	4382	<100	12641	4656	6148	9660	1707	27622	13489	18860	31117	4173
S2GDHR2-5GS-FR	<100	<100	<100	<100	<100	3065	6659	8044	5164	1072	4156	12681	14238	6453	1827	11054	31423	26556	19137	6777
S2GDHR2-5GS-E2p-L4P	<100	<100	<100	<100	<100	5778	11650	7370	16399	977	8613	14120	5999	19054	4733	13126	28298	18219	77734	12356
S2GDHR2-10GS-I3-01v9-L7P	<100	<100	<100	<100	<100	5465	5151	1440	6831	4722	14684	22060	12830	23608	13575	5373	11579	4992	11265	8772

fig. S8. SARS-CoV-2 spike/spike-NP vaccine-induced neutralizing antibody response. (A) Pseudovirus neutralization curves of mouse sera from five SARS-CoV-2 spike-based vaccine groups against two pseudoviruses, SARS-CoV-1-pp and SARS-CoV-2-pp. **(B)** Summary of ID_{50} titers measured for five SARS-CoV-2 spike-based vaccine groups against two pseudoviruses. Color coding indicates the level of ID_{50} titer (white: no binding; green to red: low to high). The ID_{50} values were calculated in GraphPad Prism 8.4.3, with the lower/upper constraints of %neutralization set at 0.0/100.0.

fig. S9

A

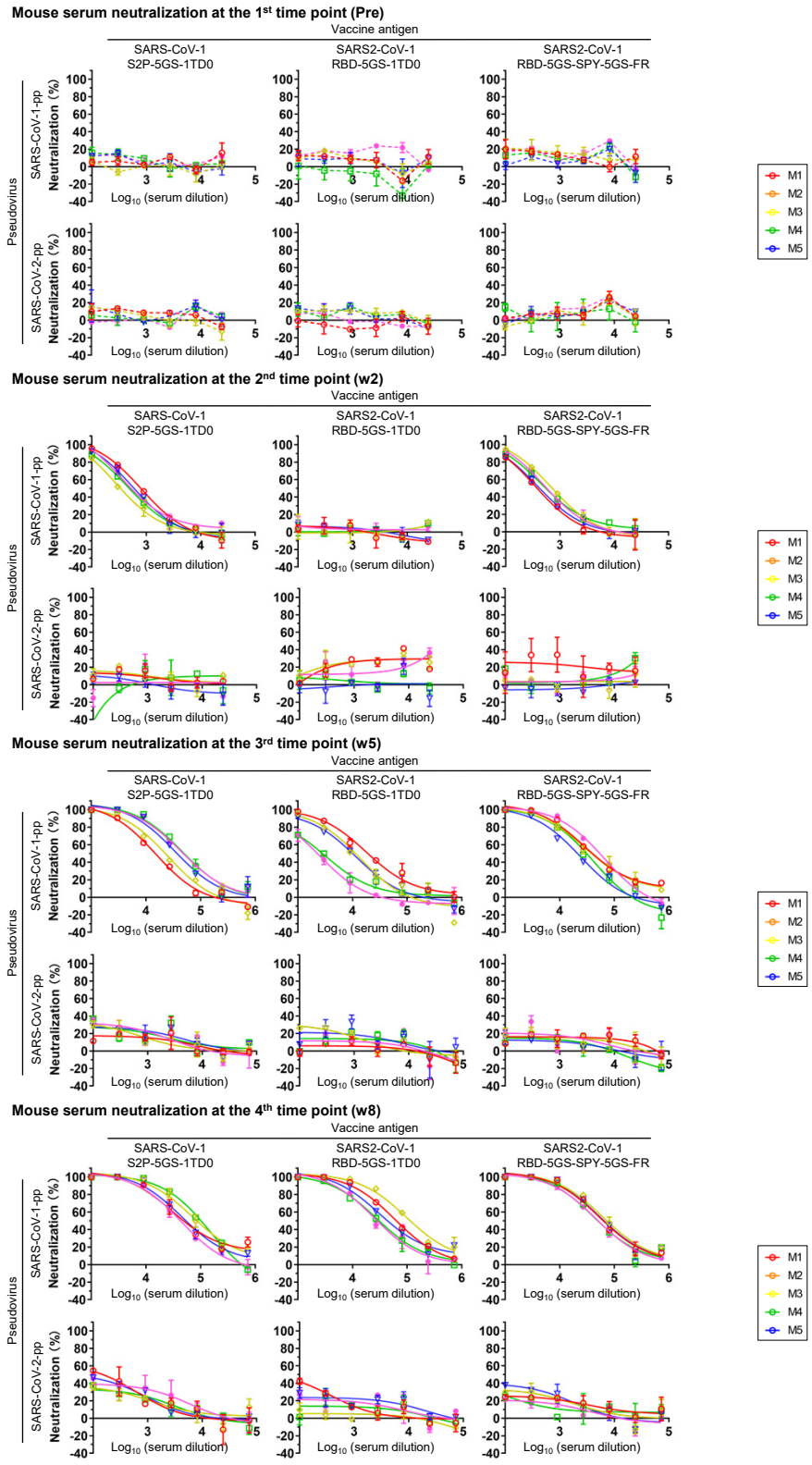

fig. S9

Mouse serum neutralization at the 5th time point (w11)

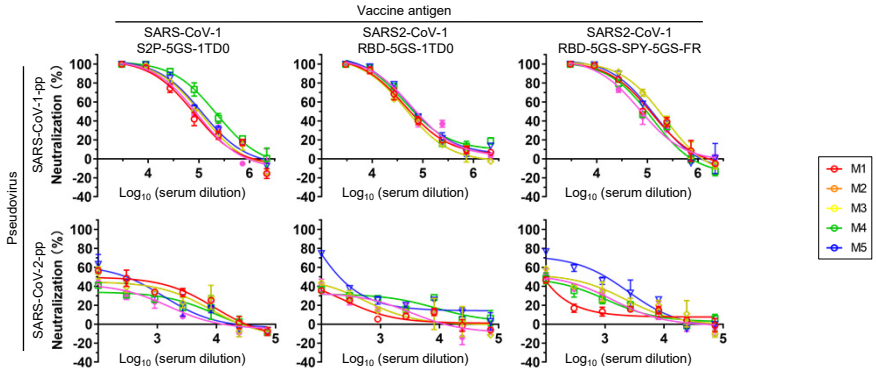

B

Mouse serum neutralization ID_{50} values

Pseudovirus	SARS-CoV-1 vaccine antigen	w2					w5					w8					w11				
		M1	M2	M3	M4	M5	M1	M2	M3	M4	M5	M1	M2	M3	M4	M5	M1	M2	M3	M4	M5
SARS-CoV-1-pp	S2P-5GS-1TD0	770	343	591	487	593	14583	21202	38507	51532	49913	56161	91290	57692	90786	42757	74328	94977	109706	198568	80619
	RBD-5GS-1TD0	<100	<100	<100	<100	<100	19980	10126	9368	2830	2110	65863	120732	49566	32475	30098	62357	52065	78969	74719	80296
	RBD-5GS-SPY-5GS-FR	370	719	423	588	584	45123	43109	19859	26996	50574	66993	77427	69400	53156	52677	109989	157931	117525	86514	77985

Pseudovirus	SARS-CoV-2 vaccine antigen	w2					w5					w8					w11				
		M1	M2	M3	M4	M5	M1	M2	M3	M4	M5	M1	M2	M3	M4	M5	M1	M2	M3	M4	M5
SARS-CoV-2-pp	S2P-5GS-1TD0	<100	<100	<100	<100	<100	<100	<100	<100	<100	<100	174	<100	142	<100	140	325	216	268	112	114
	RBD-5GS-1TD0	<100	<100	<100	<100	<100	<100	<100	<100	<100	<100	<100	<100	<100	<100	<100	<100	103	272	<100	<100
	RBD-5GS-SPY-5GS-FR	<100	<100	<100	<100	<100	<100	<100	<100	<100	<100	<100	<100	<100	<100	<100	<100	240	717	150	184

C

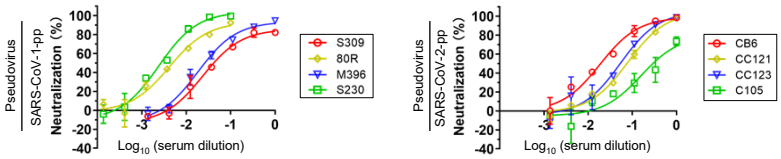

D

Mouse serum neutralization against MLV-pp at the 4th time point (w8)

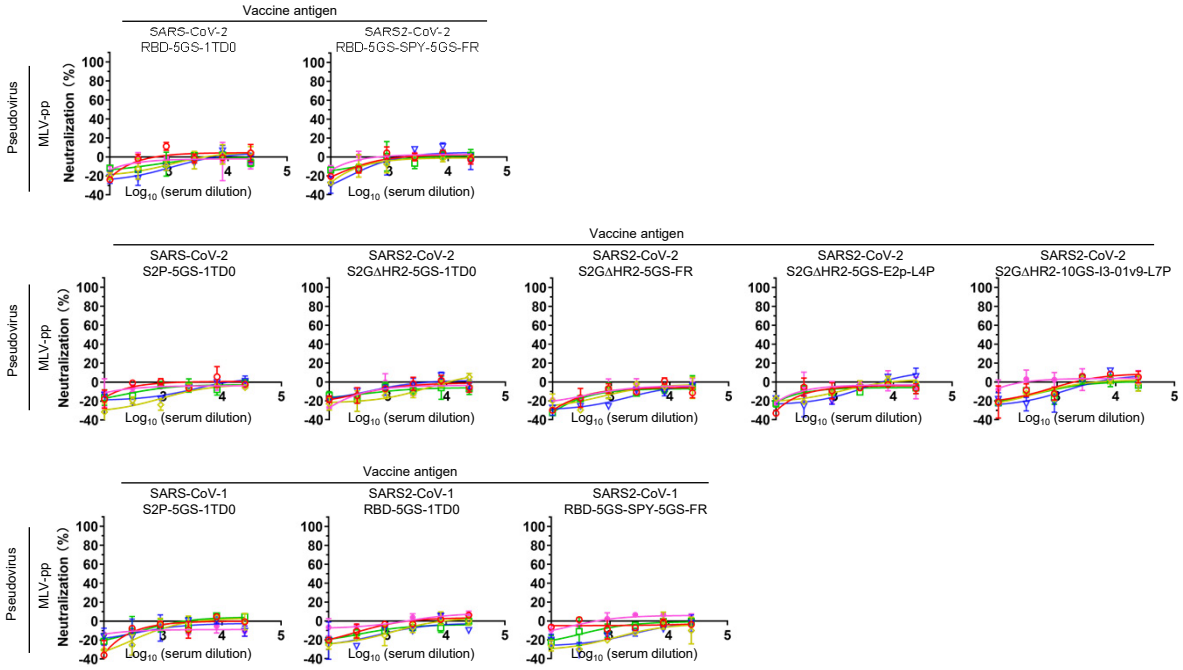

fig. S9. SARS-CoV-1 spike/RBD/RBD-NP vaccine-induced neutralizing antibody response. (A) Pseudovirus neutralization curves of mouse sera from three SARS-CoV-1 vaccine groups against two pseudoviruses, SARS-CoV-1-pp and SARS-CoV-2-pp. **(B)** Summary of ID_{50} titers measured for three SARS-CoV-1 vaccine groups against two pseudoviruses. Color coding indicates the level of ID_{50} titer (white: no binding; green to red: low to high). The ID_{50} values were calculated in GraphPad Prism 8.4.3, with the lower/upper constraints of %neutralization set at 0.0/100.0. **(C)** Pseudovirus neutralization curves of 4 known SARS-CoV-1 NAbs against SARS-CoV-1-pps (left) and 4 known SARS-CoV-2 NAbs against SARS-CoV-2-pps (right). **(D)** Pseudovirus neutralization curves of mouse sera from all vaccine groups at w8 against MLV-pps as negative control. No MLV-pp neutralization was observed.